

UNIVERSITY OF PISA
DEPARTMENT OF CIVIL ENGINEERING



A synthetic review of plunging jet scour phenomena

S. Pagliara

University of Pisa - Italy

CONTENTS

1. Part 1: Hydraulics of Plane Plunge Pool Scour (WAV)
2. Part 2: Hydraulics of 3D Plunge Pool Scour (UNIPPI)
3. Part 3: Temporal evolution of plunge pool scour (WAV)
4. Part 4: Crossing jets (UNIPPI)

1. HYDRAULICS OF PLANE PLUNG POOL SCOUR

High velocity water jet originates from the trajectory spillway dissipates its energy by causing a massive scour downstream of the dam.

In order to prevent damage to the structure it becomes necessary to foresee the scour behaviour.

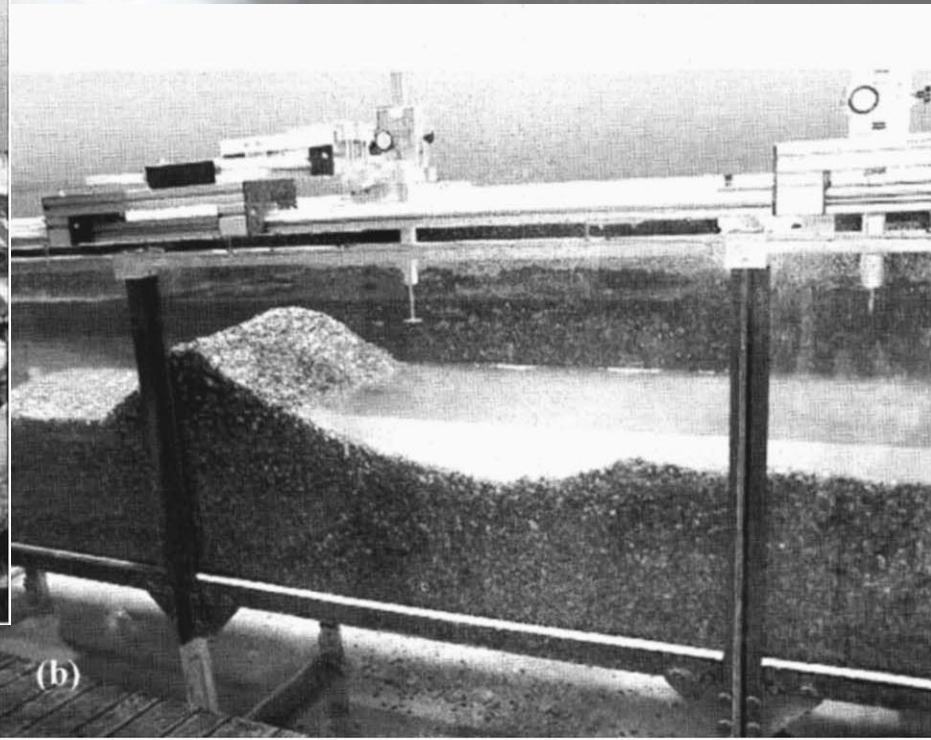
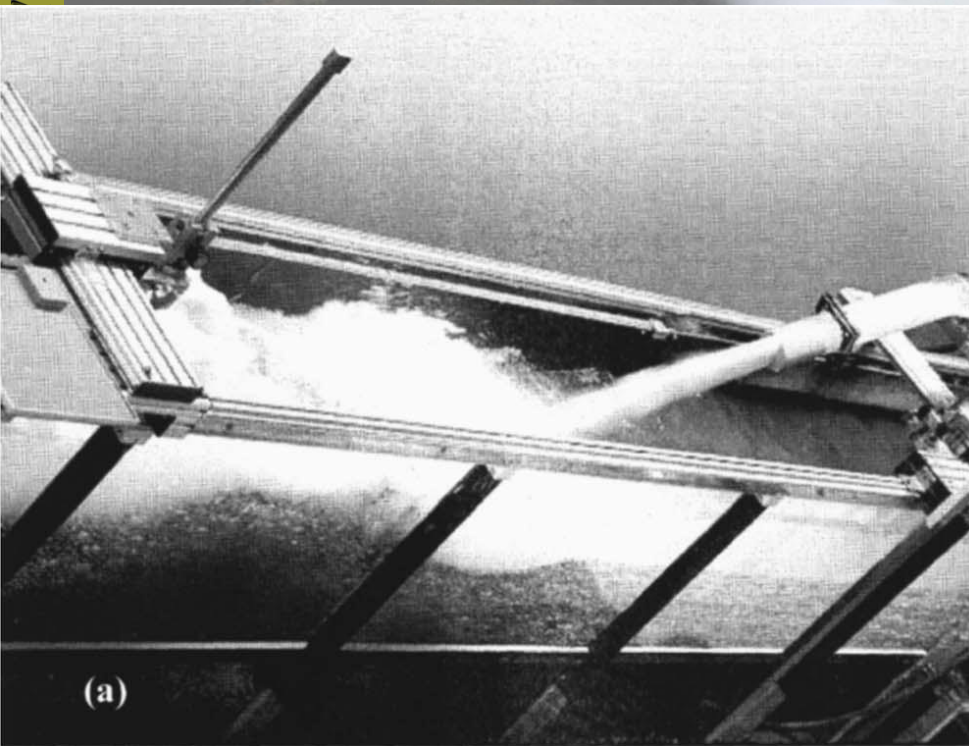


O'Shaughnessy Dam

EXPERIMENTAL APPROACH

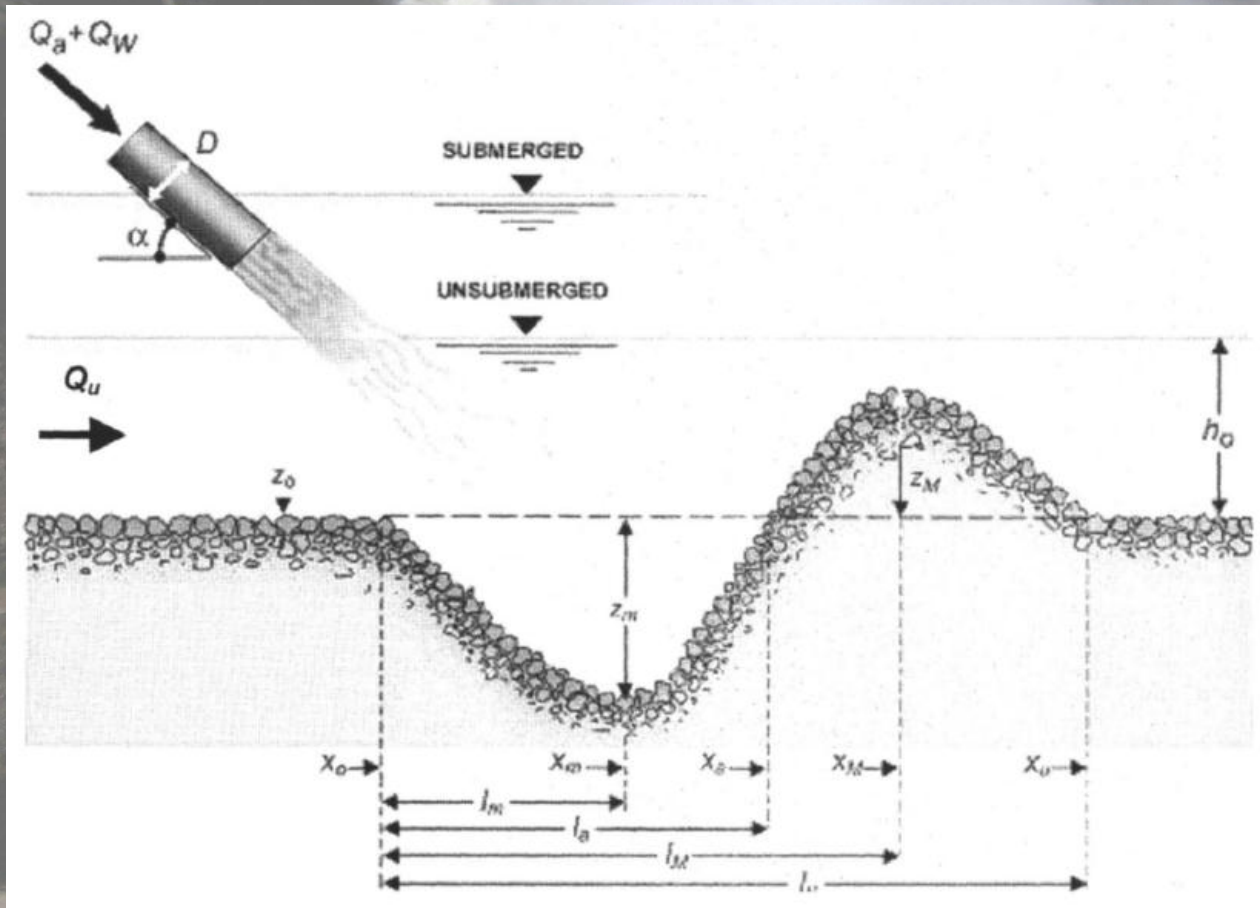
Pagliara et al (2006) conducted scour experiments in a rectangular channel previously described by Canepa and Hager 2003. Its width is 0.500 m; it is 0.70 m high and about 6 m long.

A completely disintegrated rock simulate the bed



EXPERIMENTAL APPROACH

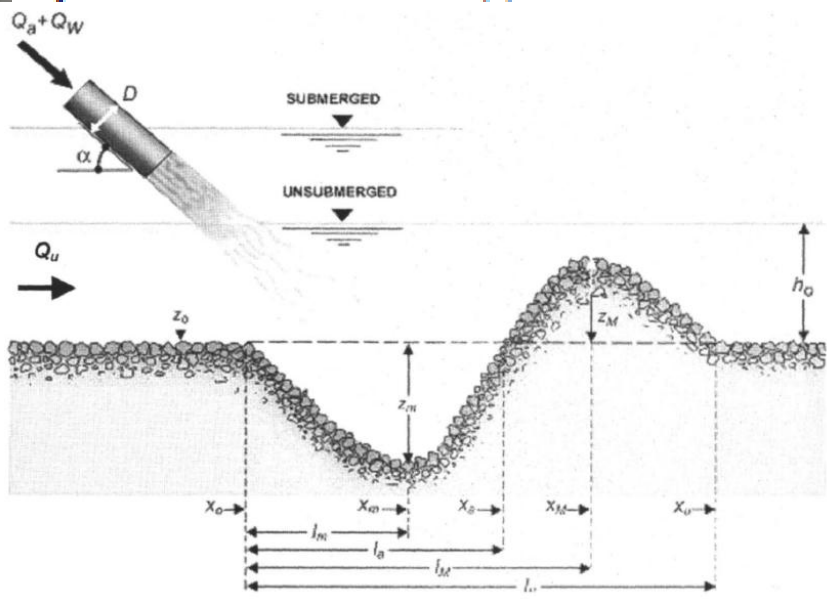
Four jet impact angles relative to the horizontal were investigated, namely, 30, 45, 60, and 90°



The usual jet shape was circular, except for a special series where jets issued from rectangular slits of 0.029 m were produced with a 0.100 m conduit, with the slit axis both horizontal and vertical. Plunge pool scour normally involves a rock bed, whose resistance against hydraulic impact is difficult to assess.

EXPERIMENTAL APPROACH (PAGLIARA ET AL, 2006)

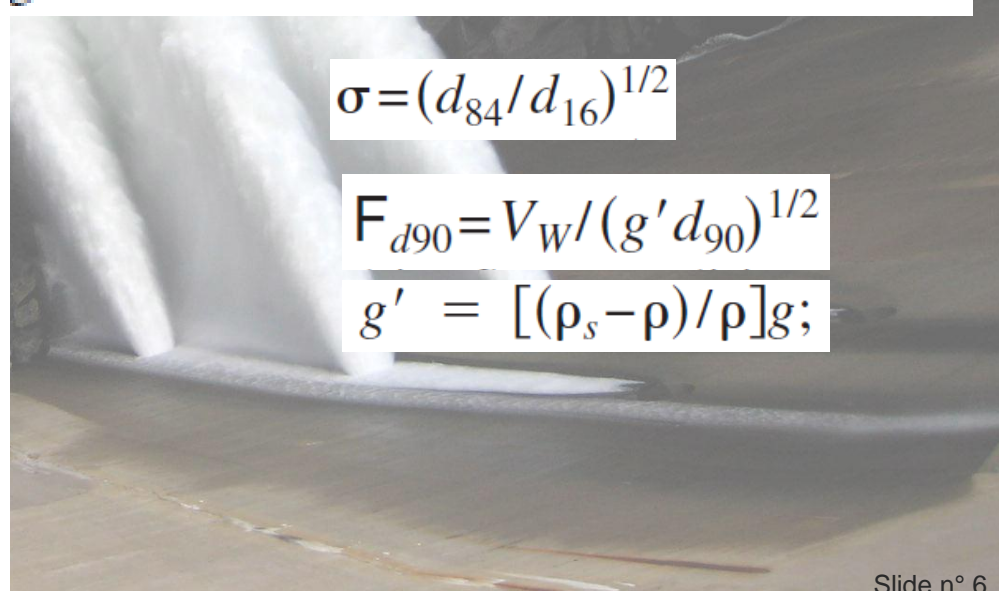
Series I and II: Series I involved almost uniform sediment characterized by $d_{16}=5.2$ mm, $d_{50}=6.5$ mm, $d_{84}=7.8$ mm, and $d_{90}=8.0$ mm, thus $\sigma=1.22$. The initial sediment thickness varied between 0.30 and 0.40 m. Water discharges were up to $Q_W=0.025$ m³/s, whereas air discharge was limited to $Q_A=0.045$ m³/s for a constant pipe diameter $D=0.070$ m. Series II involves the effects of the tailwater depth, the granulometry, the upstream velocity, and the ridge removal.



$$\sigma = (d_{84}/d_{16})^{1/2}$$

$$F_{d90} = V_W / (g' d_{90})^{1/2}$$

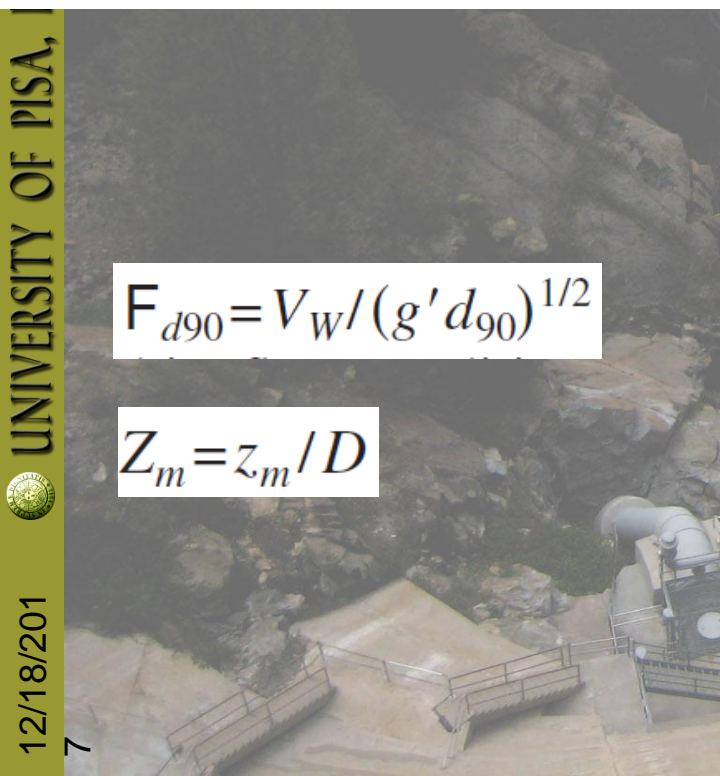
$$g' = [(\rho_s - \rho) / \rho] g;$$



Effect of Jet Shape

The effect of jet shape on the maximum scour depth is important because flip-buckets may generate a jet geometry that deviates largely from the circular shape as used in the present tests. Therefore a special series of experiments was conducted using four different jet shapes: Circular conduits of internal diameters (1) $D=0.100$ m (Canepa and Hager 2003) and (2) $D=0.070$ m; and rectangular jets (3) of width $b=0.100$ m and height $h_j=0.029$ m, and (4) inverted with $b=0.029$ m and $h_j=0.100$ m. Only black-water observations were considered because the effect of air is discussed below. The equivalent (subscript e) diameters of configurations (3) and (4) are $D_e=(4bh_j/\pi)^{1/2}=0.061$ m. The base data of Canepa and Hager (2003) were not rec they followed essentially configuration (1), as was considered too low.

APPROACH



$$F_{d90} = V_W / (g' d_{90})^{1/2}$$

$$Z_m = z_m / D$$

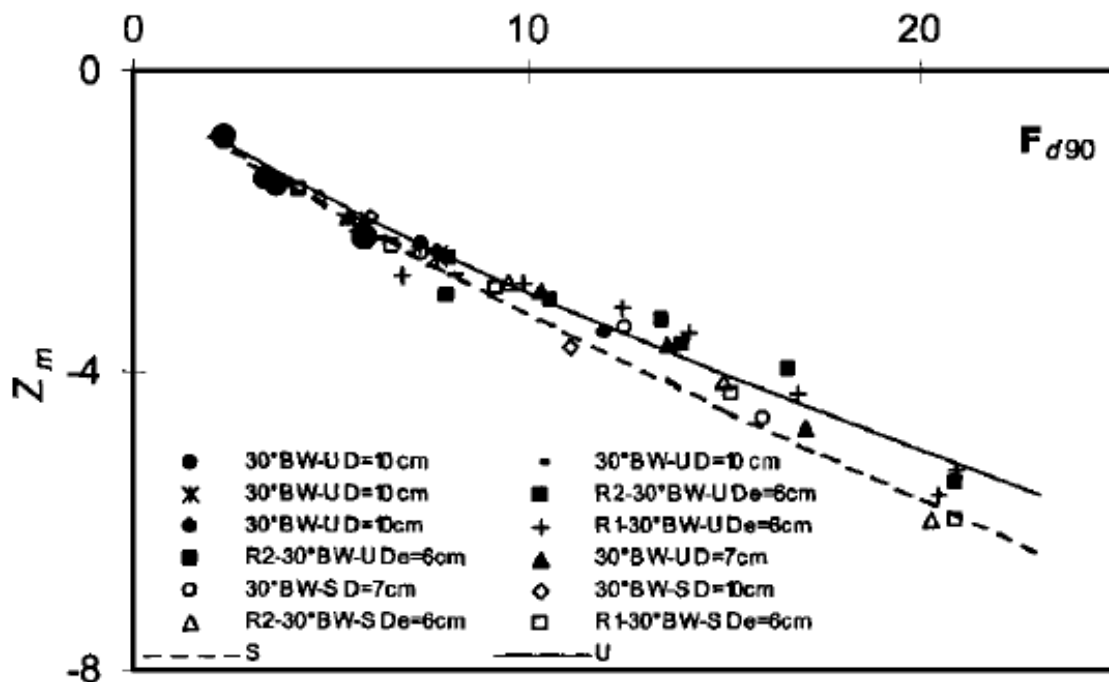


Fig. 3. Effect of jet shape on maximum scour depth $Z_m(F_{d90})$ for unsubmerged (closed symbols) and submerged jet flows (open symbols), (—) trend lines

Effect of Jet Impact Angle

The maximum scour depth Z_m may be expressed with independent functions f_1 to f_6 accounting for the main parameters of the present research as

$$Z_m = f_1(F_{d90}) \cdot f_2(\alpha) \cdot f_3(\beta) \cdot f_4(T) \cdot f_5(\sigma) \cdot f_6(F_u) \cdot f_7(S \text{ or } U) \quad (1)$$

Fig. 4 shows black-water data as $Z_{m+} = Z_m / f_2(\alpha)$ in which $f_2 = 0.38 \sin(\alpha + 22.5^\circ)$ was fitted for both submerged (S) and unsubmerged (U) flows ($f_7 = 1$) for the four jet impact angles $\alpha = 30, 45, 60,$ and 90° . The difference between the S and the U data was found negligible from a detailed data analysis. For unsubmerged jet flow, the vertical distance from the pipe outlet to the tailwater surface was of the order of $2D$. For black-water flows, scour depths are practically the same for jets impinging onto a water body and those issued below it. This important finding applies for a tailwater depth of at least 2.5 times the diameter D . The maximum scour depth for $\beta = 0$ thus is from Eq. (1)

$$Z_m = -0.38 \sin(\alpha + 22.5^\circ) F_{d90}, \quad 2 < F_d < 20$$

$$30^\circ \leq \alpha \leq 90^\circ, \quad h_o \approx 3.5D \quad (2)$$

The effect of the jet impact angle was originally assumed to follow the sine function. However, the data sets indicated that the scour depth is larger for $\alpha = 60^\circ$ than for 90° . This may be explained with two reasons: (1) the deposition height Z_M (see below) is significantly larger for a jet impact angle of $\alpha = 60^\circ$ than of 90° because less sediment is suspended in the more confined scour hole of a vertical jet; and (2) the ridge erosion is larger for 60° than for 90° jets for otherwise identical conditions.

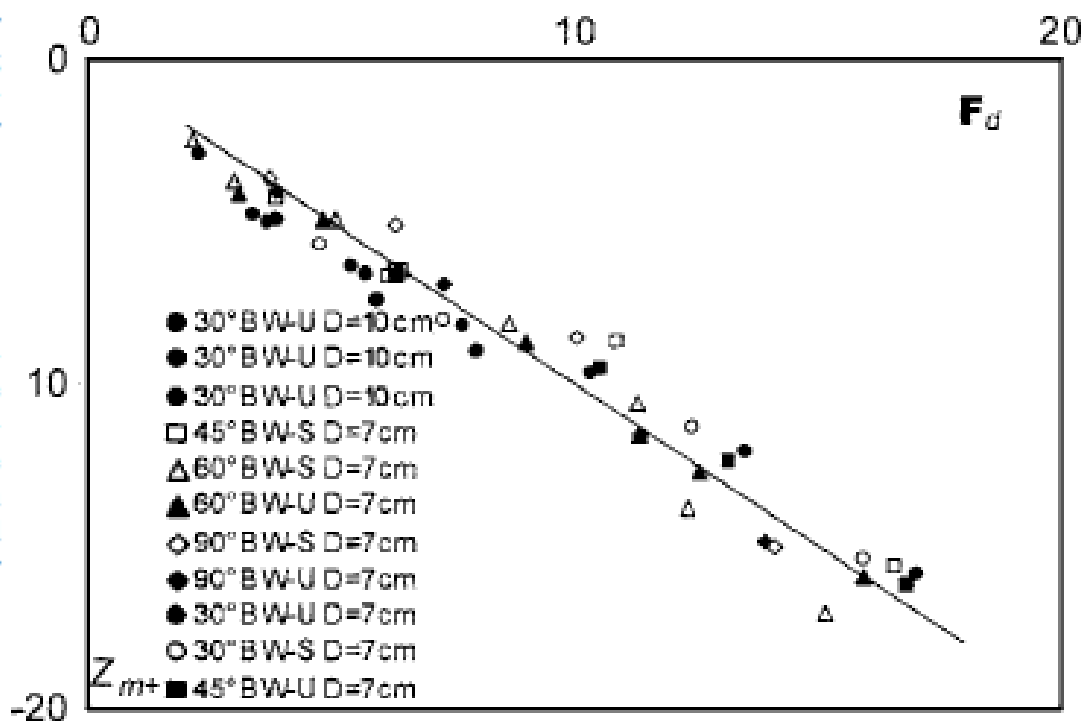


Fig. 4. Relative scour depth Z_{m+} as a function of F_{d90} for (U;S) black-water (BW) data and jet angles α between 30 and 90° ; $R^2 = 0.98$, (—) Eq. (2)



$$Z_{m+} = Z_m / f_2(\alpha)$$

EXPERIMENTAL APPROACH

Effect of Tailwater Depth

The effect of tailwater depth $T=ho/D$ was investigated for various conduit diameters D and for black-water test conditions. Two features are noted: 1) the scour depth Z_m increases linearly with the densimetric Froude number F_{d90}

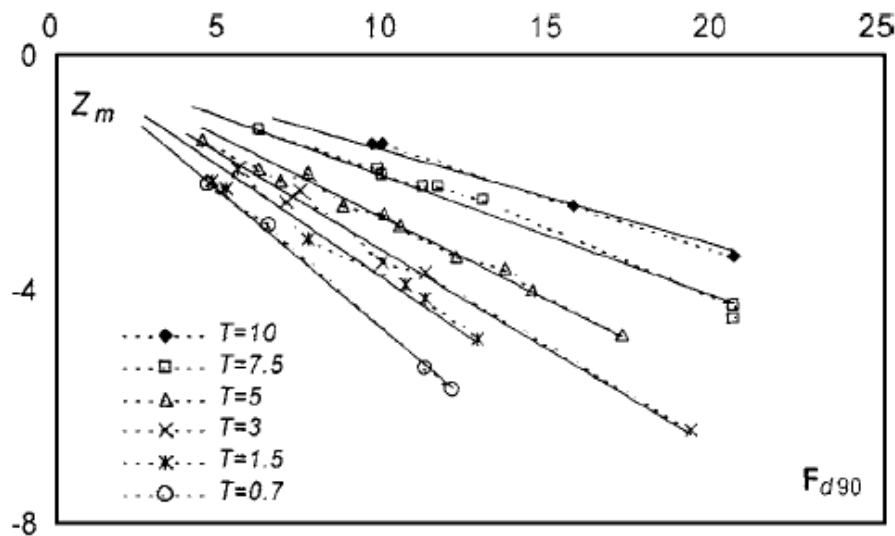


Fig. 8. Maximum scour depth $Z_m(F_{d90})$ for various tailwater depths

2) the relative scour depth Z_m decreases as relative tailwater T increases

The maximum scour depth is $Z_m = \tau F_{d90}$ where τ depends on the relative tailwater as (Fig. 8)

$$\tau = 0.12 \ln(1/T) + 0.45 \quad \text{for } 0.7 \leq T \leq 10 \quad (5)$$

Fig. 9 shows the significant tailwater effect on the scour hole geometry. For $T > 5$, the maximum scour depth (1) is comparatively small because of a relatively high ridge. For $3 < T < 4.5$, the ridge height increases to its absolute maximum (see below), associated with a small increase of the scour depth (2), because of the shorter distance between jet impingement and the scour hole. Further decreasing T to roughly 2 erodes the ridge, depending on the grain size and the water velocity in the ridge region, resulting in a deeper scour hole (3). If T is reduced to values of the order of 1, the ridge is eroded and the scour hole is unprotected (4). The erosion of the ridge may not thoroughly be analyzed with the parameters introduced herein because sediment transport depends on additional quantities. Such a discussion was considered out of the scope of this research. Note that the tests of Canepa and Hager (2003) and those of Series I were conducted in the narrow range of $3 < T < 4.5$.

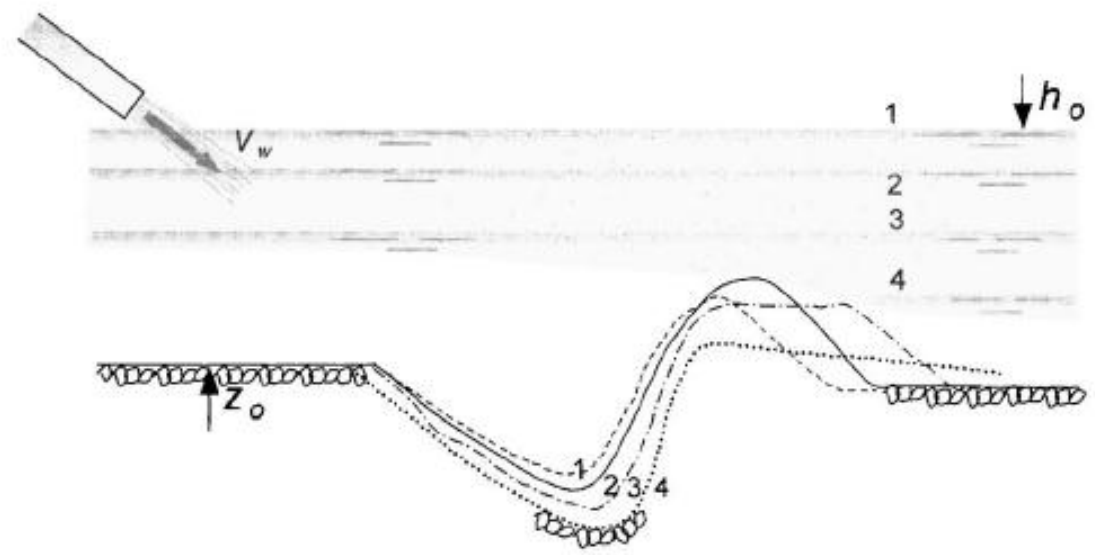
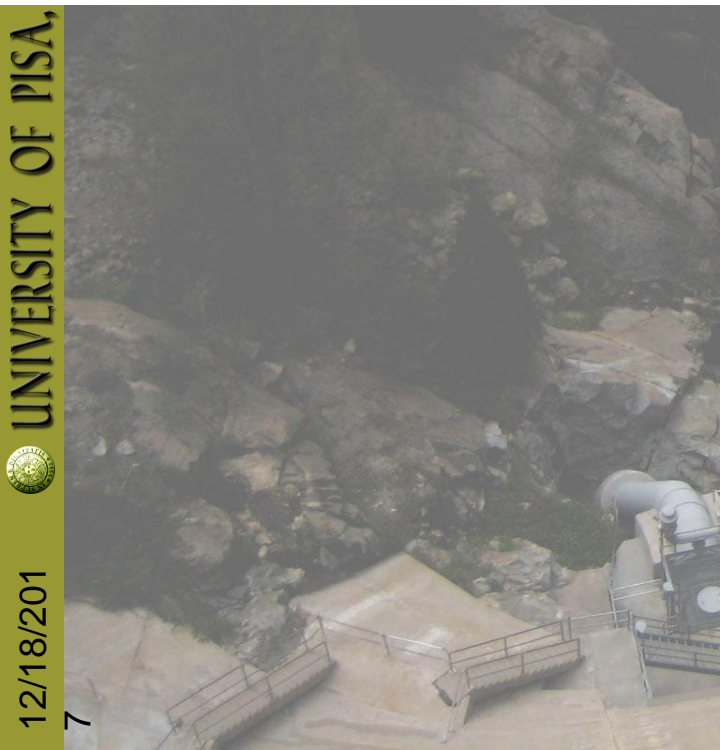
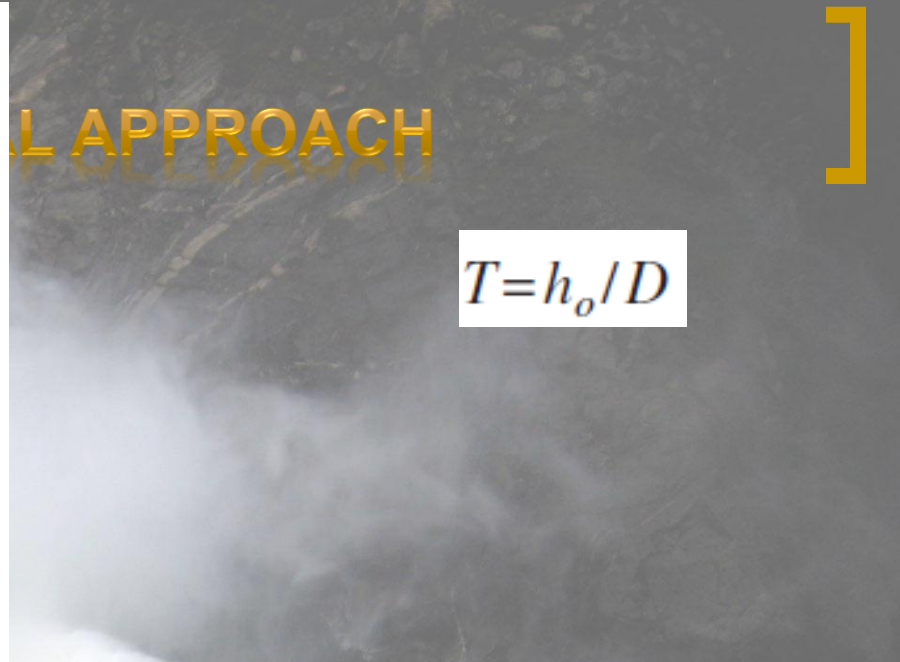


Fig. 9. Effect (schematic) of tailwater elevation on maximum scour depth and ridge height

Effect of Granulometry

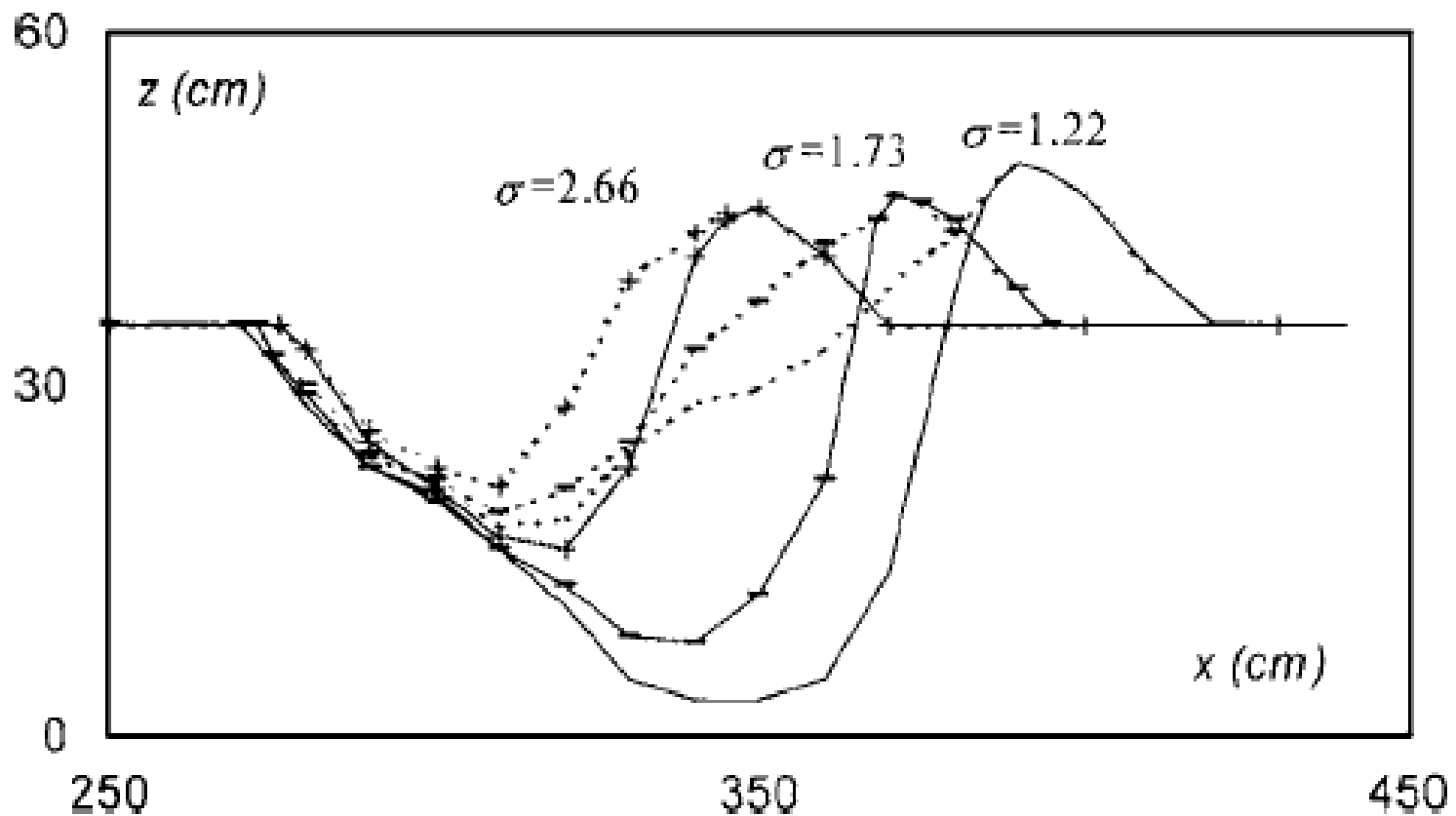


Fig. 14. Effect of sediment nonuniformity σ on scour hole geometry for $\sigma = (---)$ 1.22, $(- -)$ 1.73, $(+ +)$ 2.66, and $(—)$ dynamic and $(- -)$ corresponding static scour conditions

$$\sigma = (d_{84}/d_{16})^{1/2}$$

Ridge Removal

In special tests the sediment ridge (subscript r) was constantly removed during an experiment to provide a horizontal sediment surface downstream of the scour hole, to explore whether the scour increases. As mentioned, a ridge protects a scour hole from

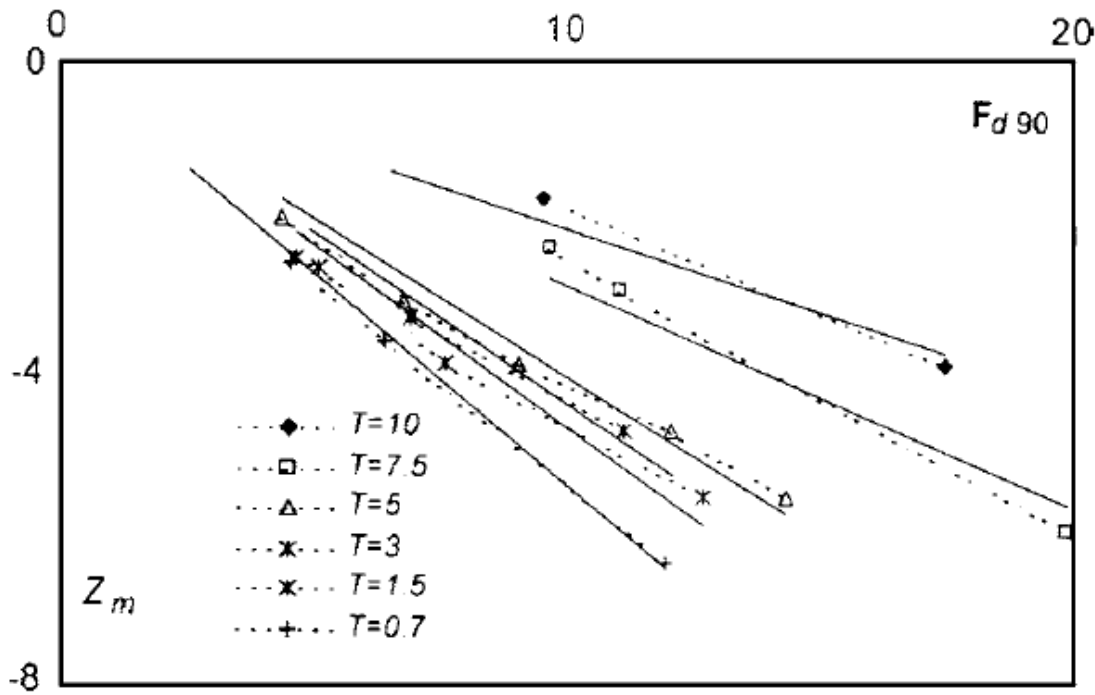
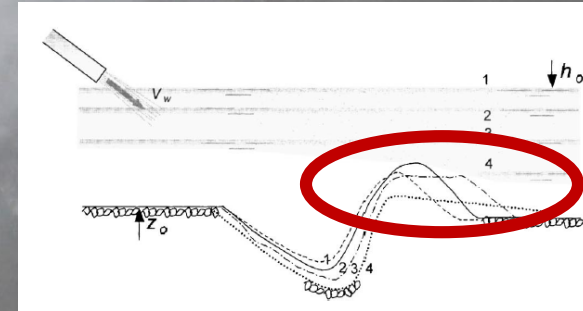


Fig. 12. Effect of ridge removal on $Z_m(F_{d90})$ (—) prediction, (- -) data lines, $3 \leq T \leq 4.5$



$$\tau = 0.12 \ln(1/T) + C_r \quad \text{for } T^{-1} > 0.05 \quad (9)$$

with $C_r = 0.45$ for ridge presence, and $C_r = 0.52$ for artificial ridge removal.

Effect of Upstream Velocity

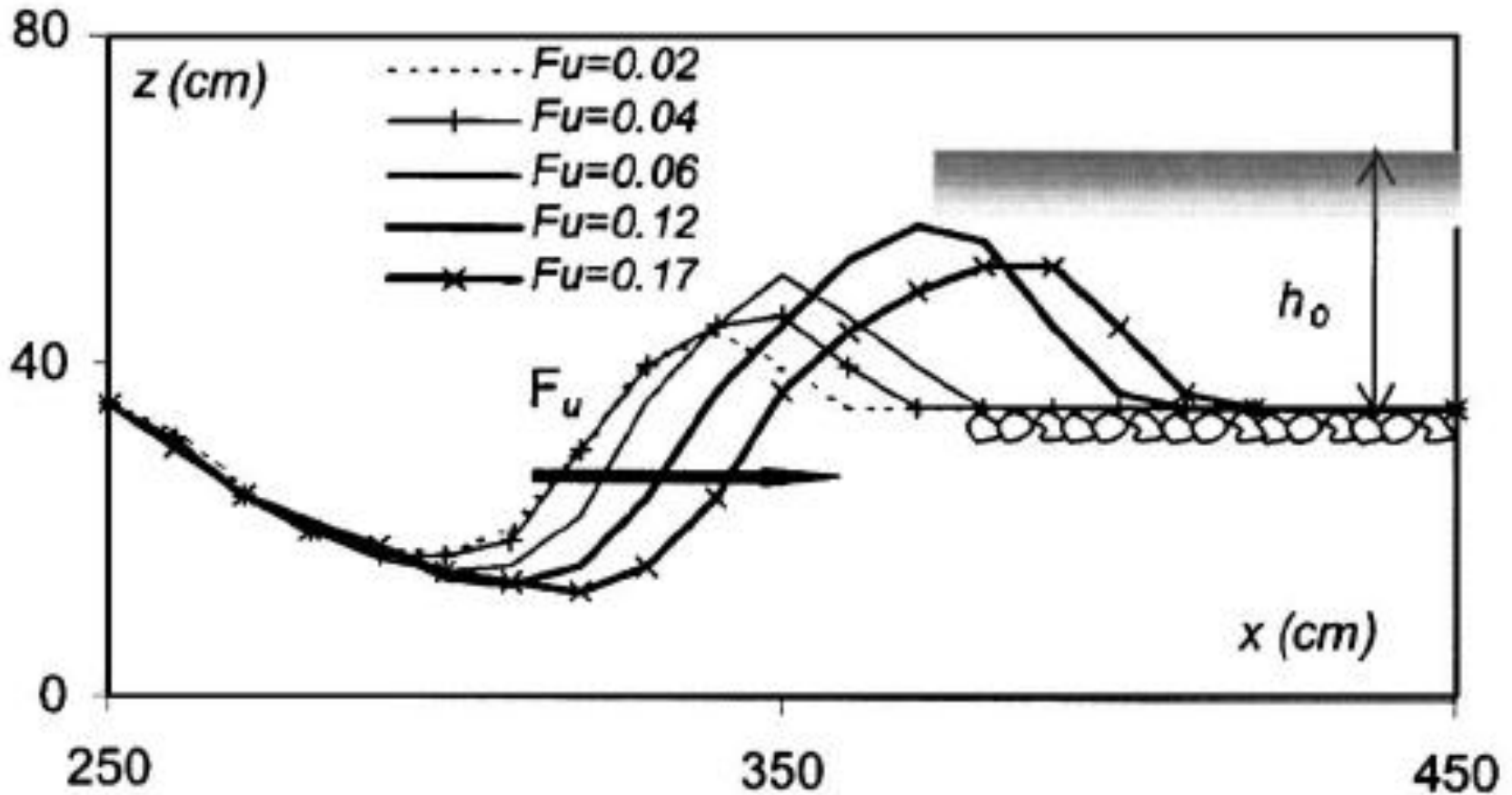


Fig. 15. Effect of upstream Froude number F_u on scour hole profile $z(x)$

General Equation for Maximum Depth of Scour Hole

Based on Canepa and Hager (2003) and the present research, the effects of all independent parameters influencing the maximum scour depth $Z_m = z_m/D$ can be assessed with

$$\text{Densimetric Froude number } F_d = V_W / (g' d_{90})^{1/2}, \quad f_1(F_d) = F_d \quad (10)$$

$$\text{Jet impact angle } \alpha, \quad f_2(\alpha) = - [0.38 \sin(\alpha + 22.5^\circ)] \quad (11)$$

$$\text{Jet air entrainment } \beta, \quad f_3(\beta) = (1 + \beta)^{-m} \quad (12)$$

$$\text{Tailwater effect } T, \quad f_4(T) = [0.12 \ln(1/T) + C_r] / 0.30 \quad (13)$$

$$\text{Sediment nonuniformity } \sigma, \quad f_5(\sigma) = - [0.33 + 0.57\sigma] \quad (14)$$

$$\text{Upstream flow effect } F_u, \quad f_6(F_u) = 1 + F_u^{0.50} \quad (15)$$

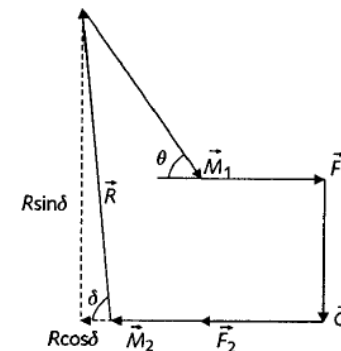
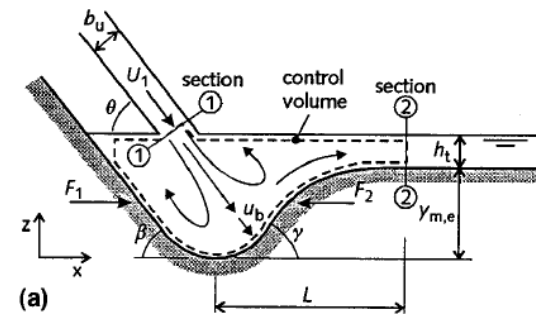
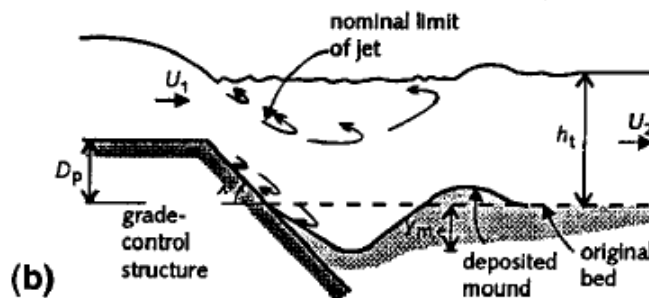
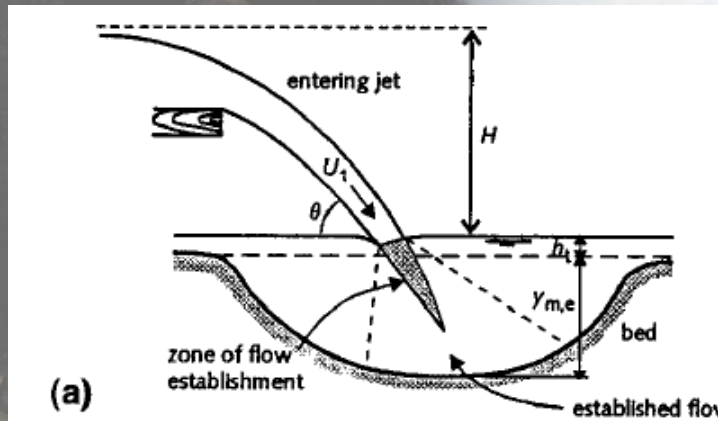
The final expression for the maximum depth of a plunge pool scour thus is

$$Z_m = f_1(F_d) \cdot f_2(\alpha) \cdot f_3(\beta) \cdot f_4(T) \cdot f_5(\sigma) \cdot f_6(F_u)$$

THEORETICAL APPROACH (HOFFMANS 1998)

The term "plunging jets" refers to jets of water that impinge on the free surface due to the discharge from an outlet above the free surface or overflow through an opening.

The forces and momentum fluxes acting on this volume are the momentum flux ($M1$) in the jet (section 1), the momentum flux ($M2$) at the outflow section (section 2), hydrostatic forces ($F1$ and $F2$), the weight of the water (G), and the resultant or dynamic force (R) exerted by the jet on the bed of the scour hole.



$$(R \cos \delta \approx F_{d,h})$$

2. Hydraulics of 3D Plunge Pool Scour

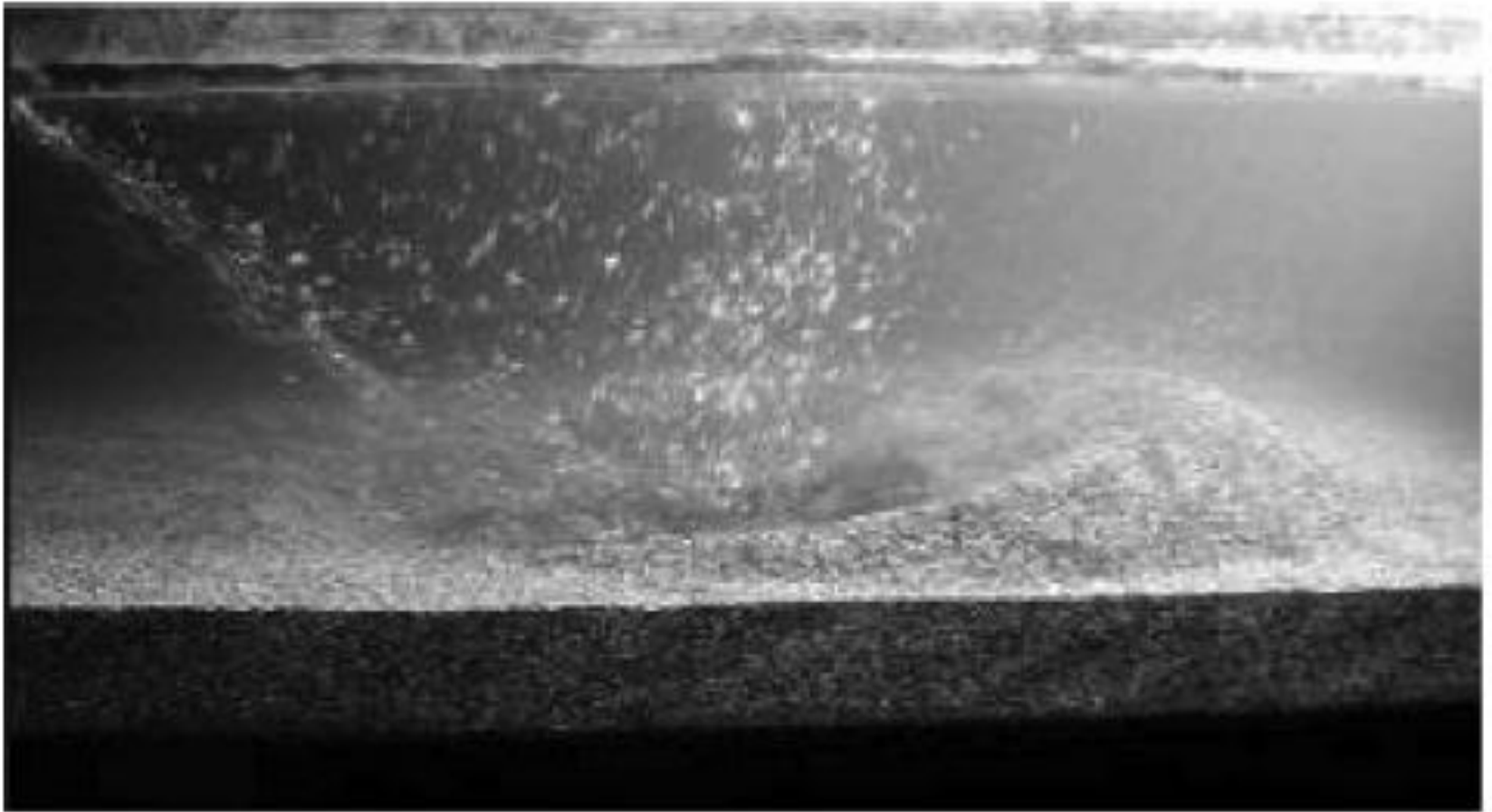


Fig. 1. View of 3D plunge pool for free jet flow ($\alpha=30^\circ$)

2. Hydraulics of 3D Plunge Pool Scour

Classification of 3D Scour Holes

The features of a 3D plunge pool scour hole are more complex than those of the 2D configuration. The jet impinging onto the sediment bed results essentially in a radial flow from the impact point with major momentum components directed laterally to the approach flow direction. Secondary currents are set up that have been barely described in previous

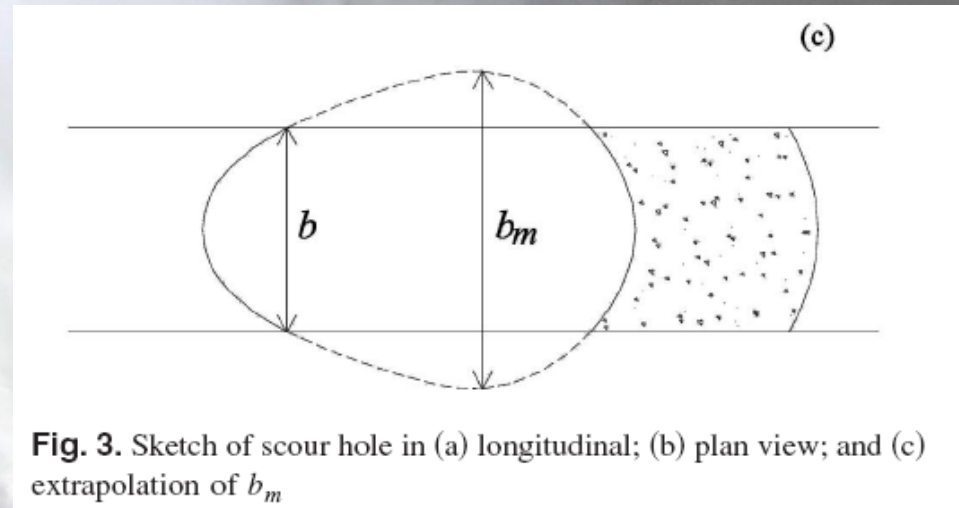
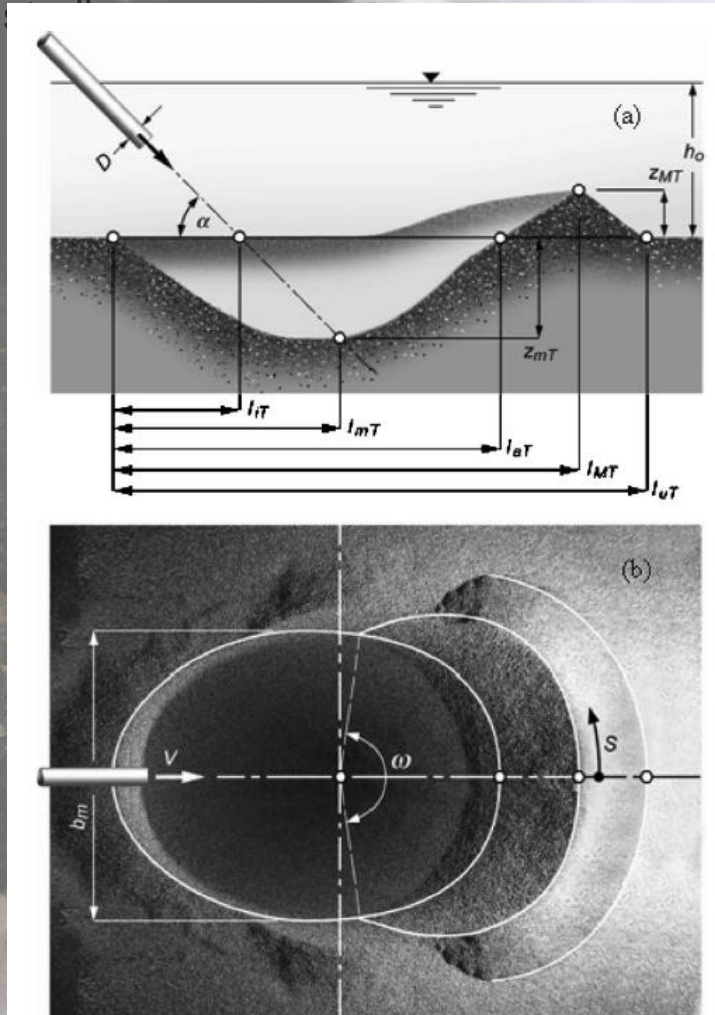


Fig. 3. Sketch of scour hole in (a) longitudinal; (b) plan view; and (c) extrapolation of b_m

$$\lambda = b_m / b$$



Table 1. Classification
Also with Fig. 2)

Type

$H_{Tw}L_\alpha$

Maximum
with the ri
height is l
direction o

$H_{Tw}I_\alpha$

Scour activ
than for H
the ridge i
hole sides.
tendency t

$H_{Tw}H_\alpha$

Scour hole tends to be circular shape along with a
reduction of the scour depth. The flow direction over the
scour hole is no more axial and the water flows more
radially from the jet impact zone.

$L_{Tw}L_\alpha$

With a tailwater reduction, the scour hole is less
developed and has an almost circular plan shape. The flow
direction from the impact zone is radially outwards.

$L_{Tw}H_\alpha$

All flow characteristics previously described are amplified,
in addition to a flow portion deflected in the direction
against the jet flow. For vertical jets, almost circular scour
holes result.

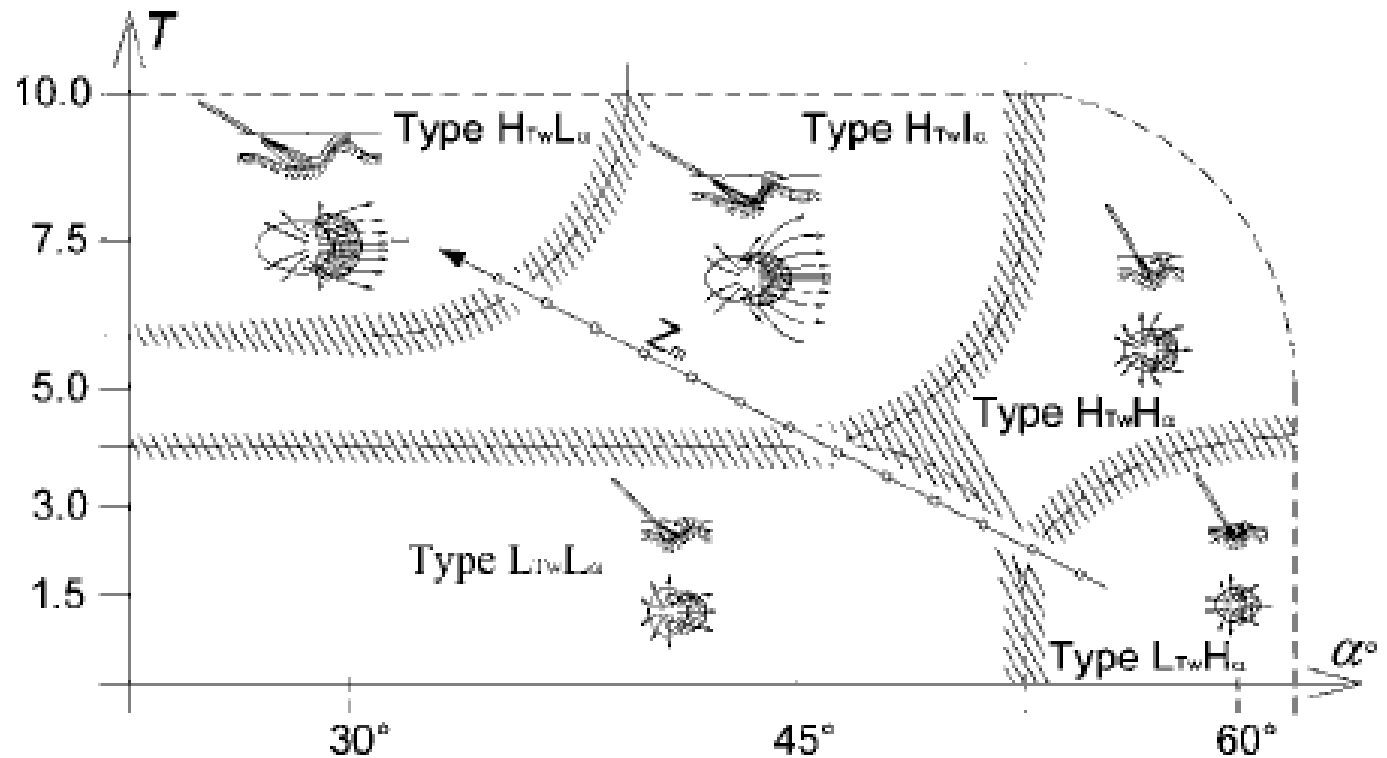
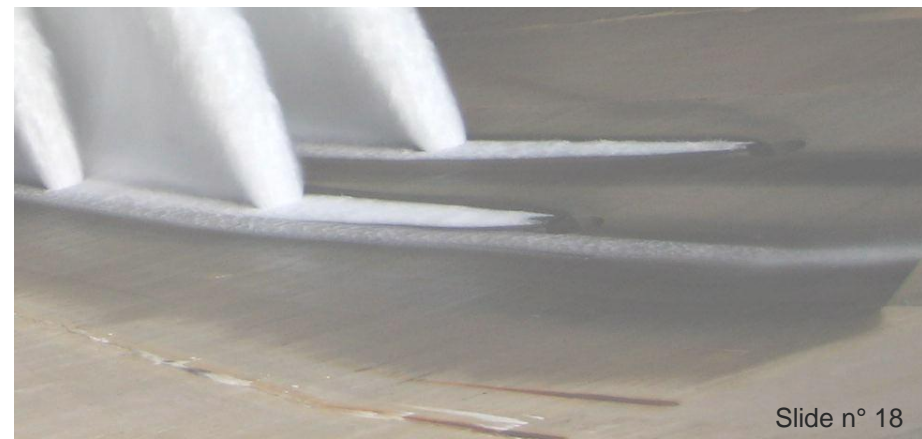


Fig. 2. Types of 3D plunge pool scour as function of impact angle α° and relative tailwater T



2. Hydraulics of 3D Plunge Pool Scour

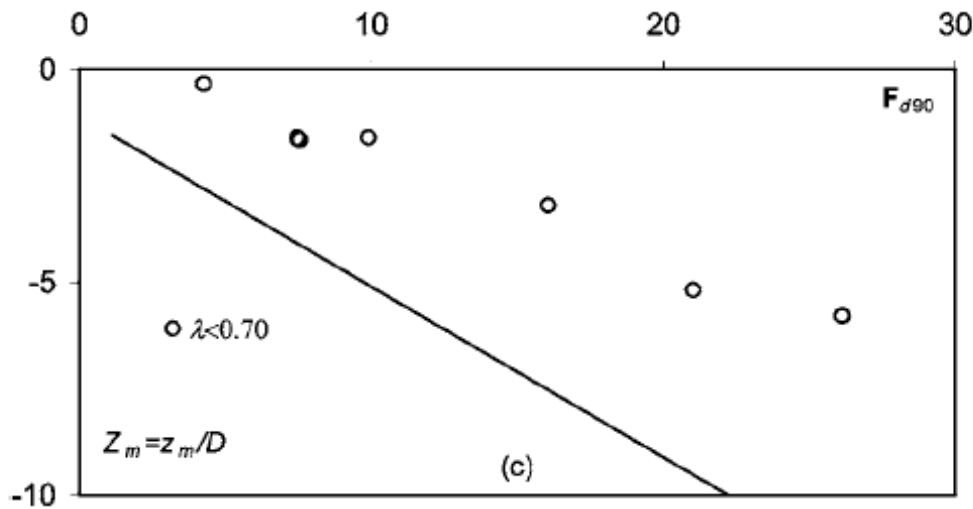
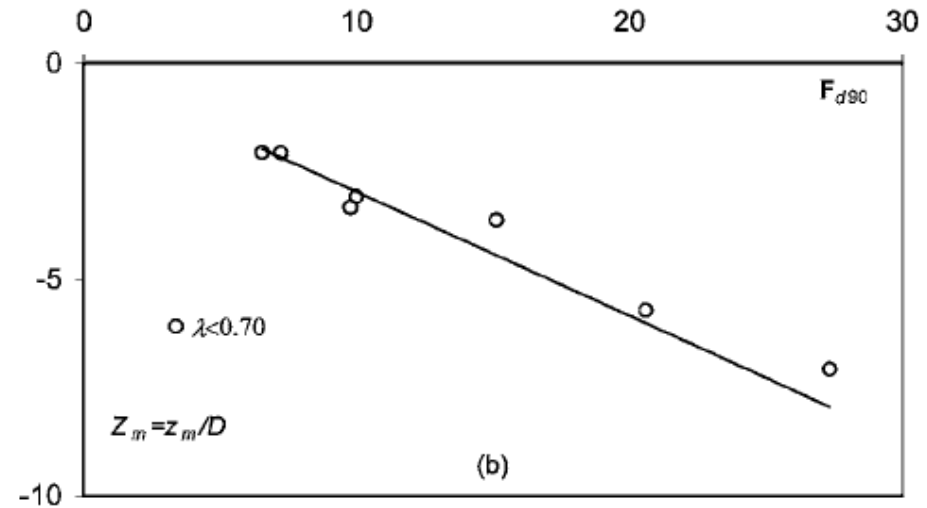
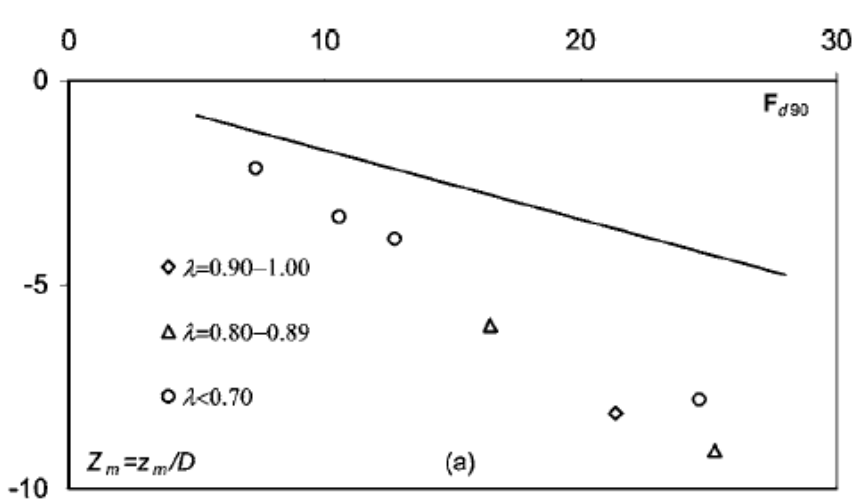
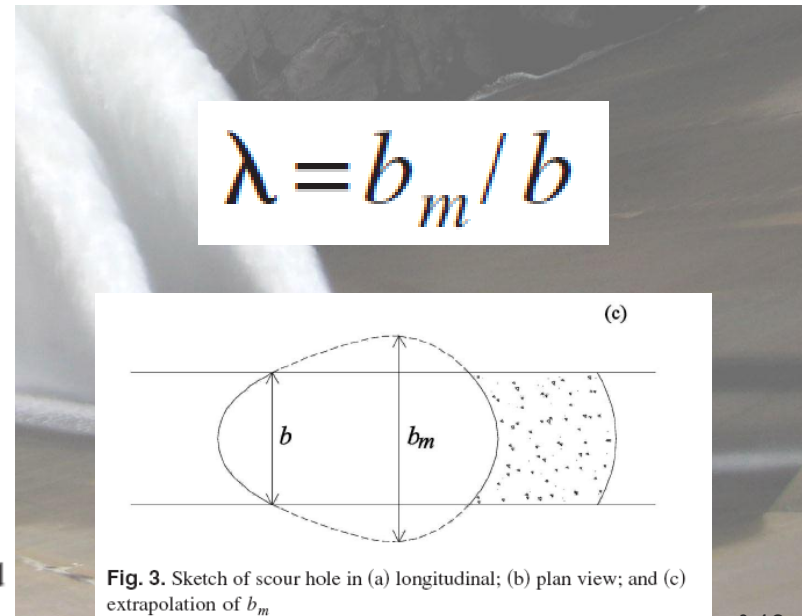


Fig. 4. Z_m versus F_{d90} for (a) $T=10$, $\alpha=30^\circ$; (b) $T=5$, $\alpha=45^\circ$; and (c) $T=1$, $\alpha=60^\circ$; (line) 2D scour (Pagliara et al. 2006)



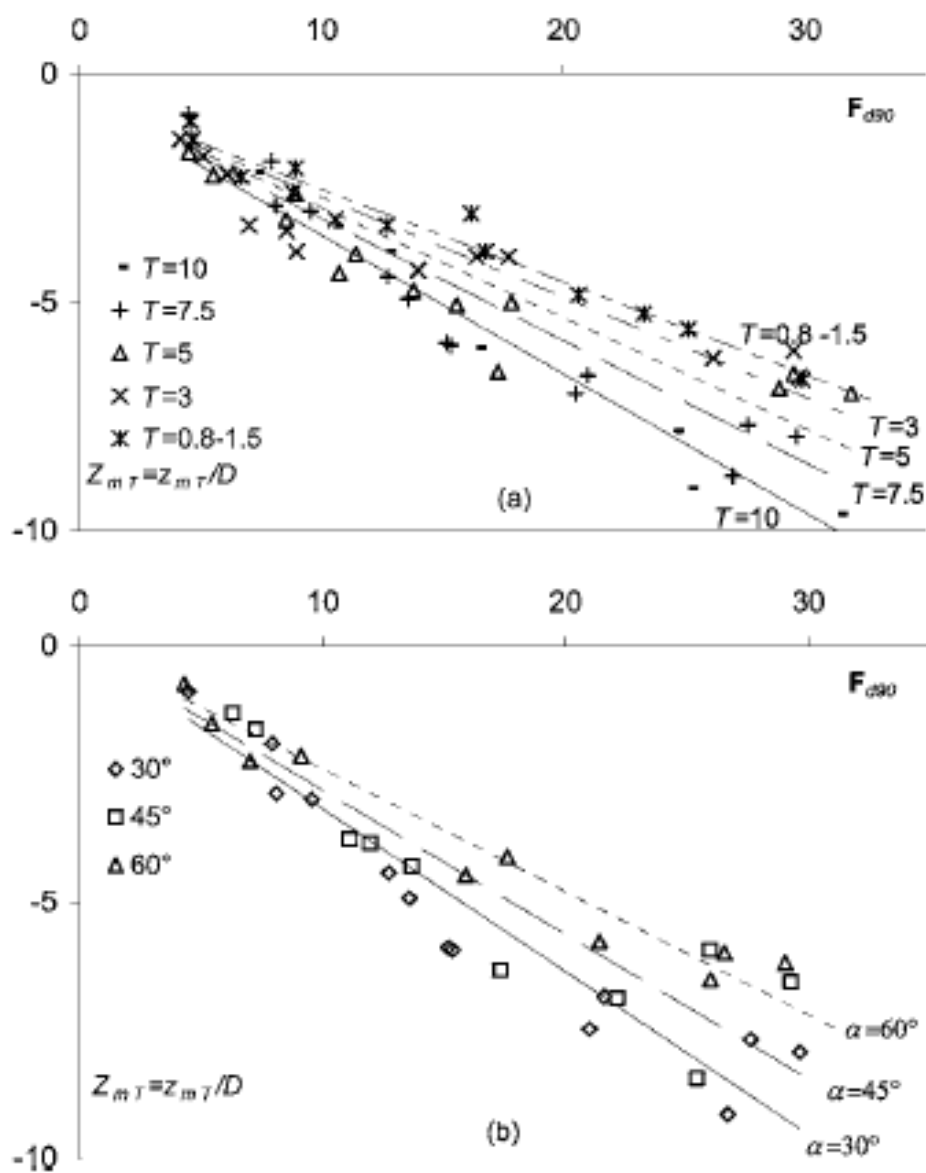


Fig. 5. (a) Tailwater effect for 3D scour for $\lambda \leq 1.50$, expressed as Z_{mT} versus F_{d90} for $\alpha = 30^\circ$; (b) jet angle effect on Z_{mT} for $T = 7.5$



Fig. 5(a) shows the maximum 3D scour depths $Z_{mT}(F_{d90})$ for $\alpha = 30^\circ$ and a variable relative tailwater submergence T . The plot confirms that as larger T , the deeper is Z_{mT} . In contrast, Z_m is inversely related to T in the scour depth equation proposed by Pagliara et al. (2006) for 2D scour. Note that the relation between Z_{mT} and F_{d90} is practically linear. Fig. 5(b) shows the relation $Z_{mT}(F_{d90})$ for the three jet impact angles $\alpha = 30, 45$, and 60° : The smaller the jet angle α , the deeper the scour hole. This effect has to do with the modified ridge geometry. Whereas the ridge in the 2D case resulted in deeper scour holes for large angles α , the partial ridge geometry in the 3D scour hole retains less suspended sediment. Fig. 6 also indicates a larger scour surface for a small jet angle as compared to large values of α .

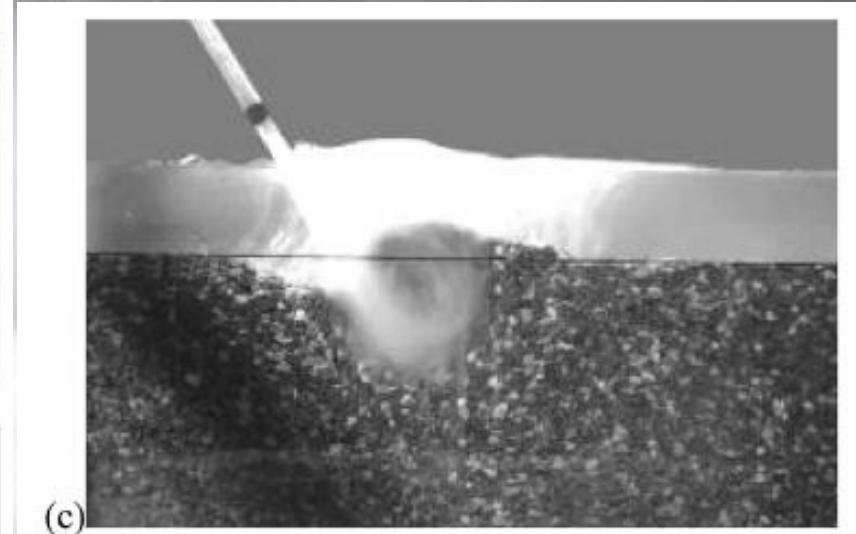
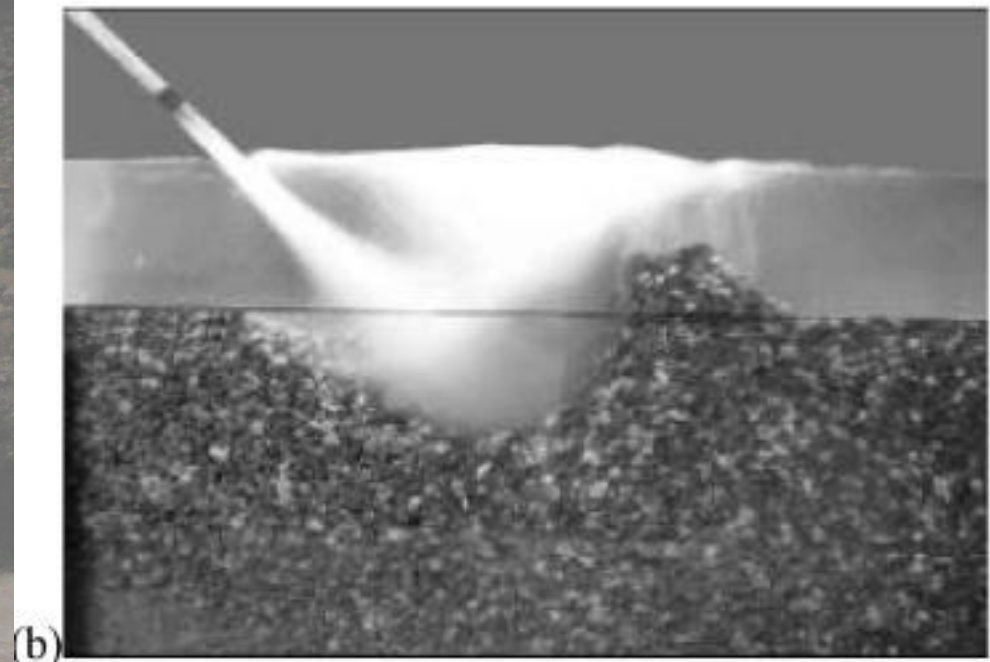
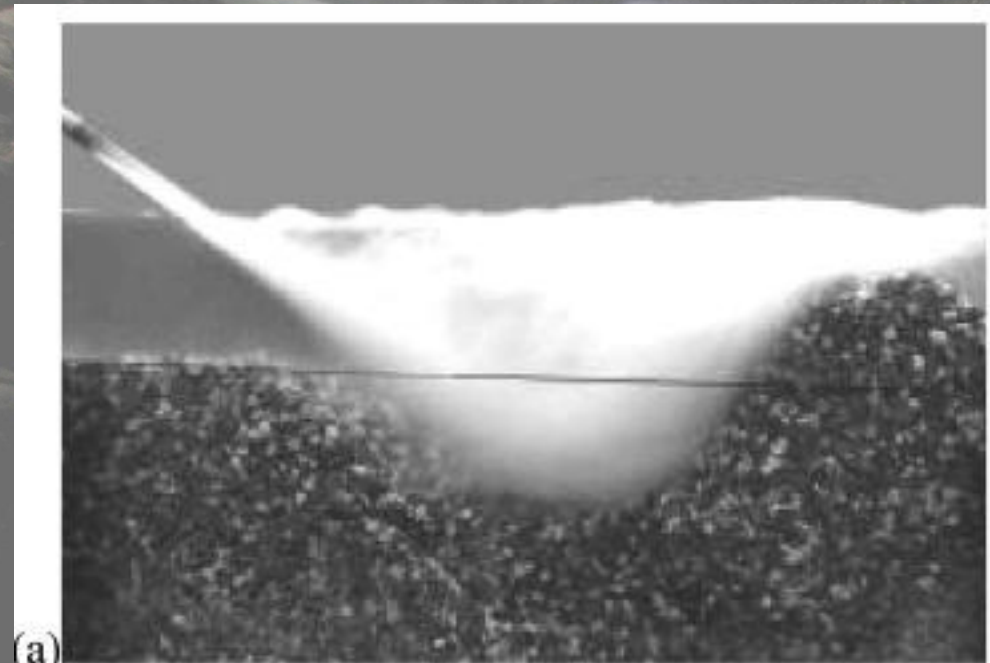
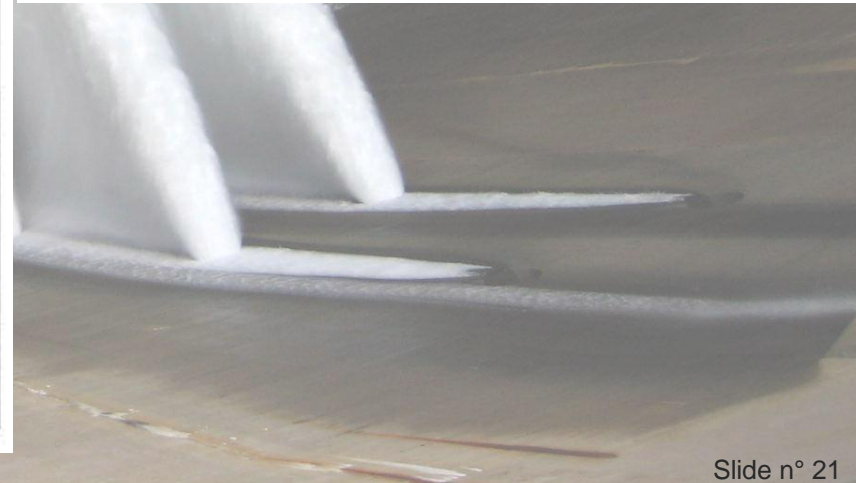


Fig. 6. Axial scour hole profiles for $T=10$ and $\alpha=$ (a) 30° ; (b) 45° ; and (c) 60° for otherwise identical flow conditions



2. Hydraulics of 3D Plunge Pool Scour

Equation for Scour Depth

Pagliari et al. (2006) proposed the following relationship for the maximum 2D scour hole depth:

$$Z_m = -f_1(F_{d90})f_2(\alpha^\circ)f_3(\beta)f_4(T)f_5(\sigma)f_6(F_u) \quad (1)$$

The individual functions f account for the effects of

Densimetric Froude number, $f_1(F_{d90}) = F_{d90} \quad (2)$

Impact jet angle, $f_2(\alpha) = [-0.38 \sin(\alpha + 22.5^\circ)] \quad (3)$

Jet air content, $f_3(\beta) = (1 + \beta)^{-0.75} \quad (4)$

Tailwater, $f_4(T) = (1/0.30)[0.12 \ln(1/T) + 0.45] \quad (5)$

Granulometry, $f_5(\sigma) = -(0.57\sigma + 0.33) \quad (6)$

Approach flow, $f_6(F_u) = (1 + F_u^{0.50}) \quad (7)$

2. Hydraulics of 3D Plunge Pool Scour

The expanded equation (1) for the maximum depth of a 3D scour hole

$$Z_{mT} = -f_1(F_{d90})f_2(\alpha)f_3(\beta)f_4(T)f_5(\sigma)f_6(F_w)f_7(\lambda)f_8(\alpha)f_9(T) \quad (11)$$

applies for both 2D and 3D scour holes with $f_7(\lambda)f_8(\alpha)f_9(T) = 1$ for $\lambda > 3.0$; and with Eqs. (8)–(10) for $\lambda \leq 1.50$ along with a linear interpolation between the two for $1.50 < \lambda < 3.0$. Eq. (11) is subject to the limitations: (1) $0.8 \leq T \leq 10$; (2) $30^\circ \leq \alpha \leq 60^\circ$; (3) $4 \leq F_{d90} \leq 30$; and (4) $\lambda \geq 0.20$, in addition to the limitations for the 2D scour equation. Fig. 8 compares the predictions with the observations and demonstrates a reasonable agreement of the data within the margins of essentially $\pm 20\%$. In the intermediate range $1.50 < \lambda < 3.00$, a linear interpolation was applied (see the following).

2. Hydraulics of 3D Plunge Pool Scour

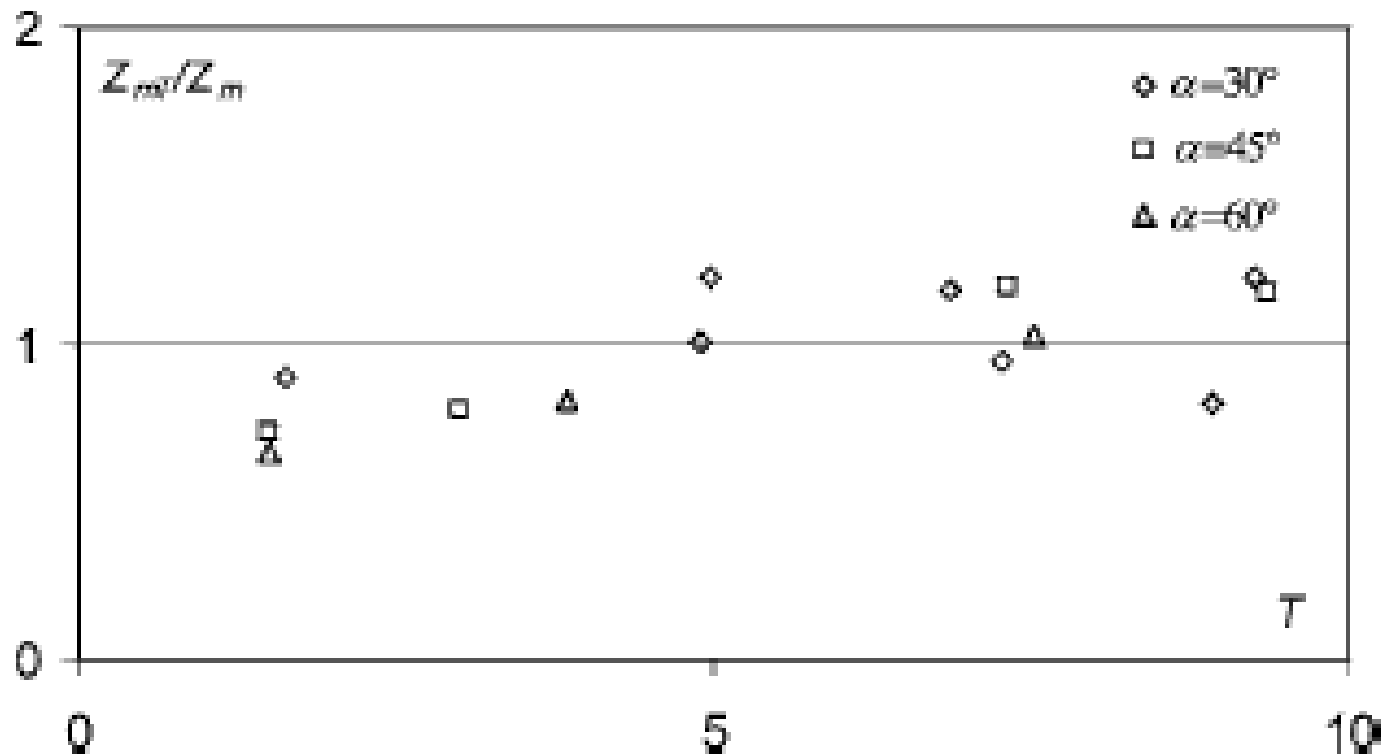


Fig. 7. Function $Z_{mT}/Z_m(T)$ for $2.5 < \lambda < 3$ and $30^\circ \leq \alpha \leq 60^\circ$ demonstrating a quasi-2D scour depth

2. Hydraulics of 3D Plunge Pool Scour

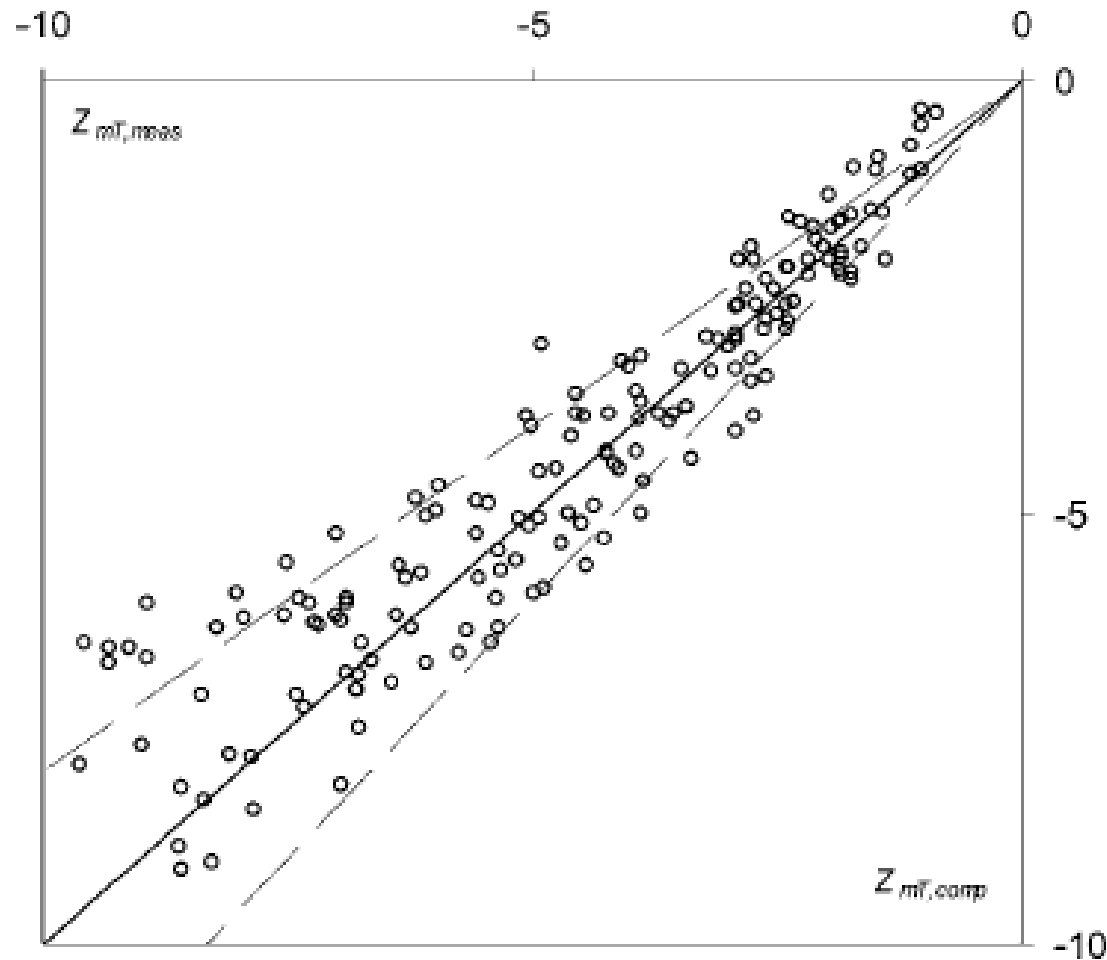


Fig. 8. Maximum scour depth of 3D scour hole Z_{mT} computed and measured, with $\pm 20\%$ lines

Static vs dynamic maximum scour

Maximum Static Scour Depth

a distinctive difference exists between the “static” and the “dynamic” scour holes. The static scour hole applies to conditions when the jet flow is stopped after a test, whereas the dynamic scour hole corresponds to conditions with the jet flow turned on. The latter may not be observed in prototypes whereas static scour holes may be surveyed after a flood.

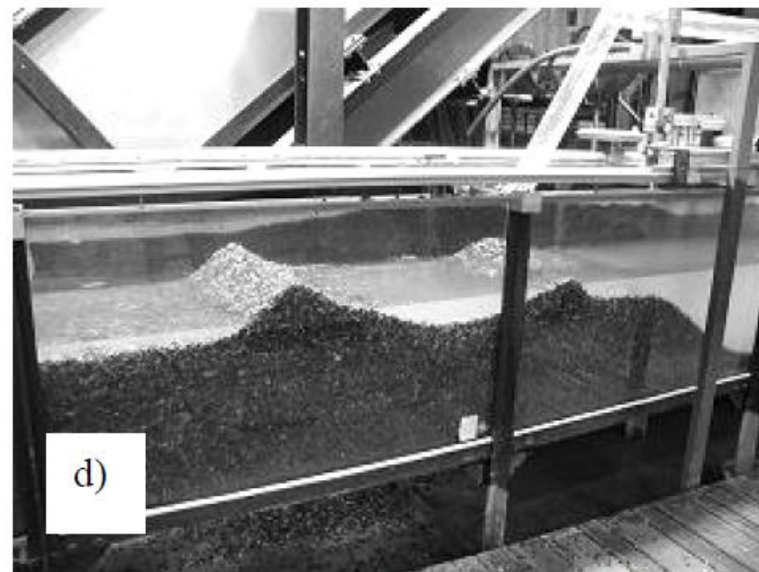
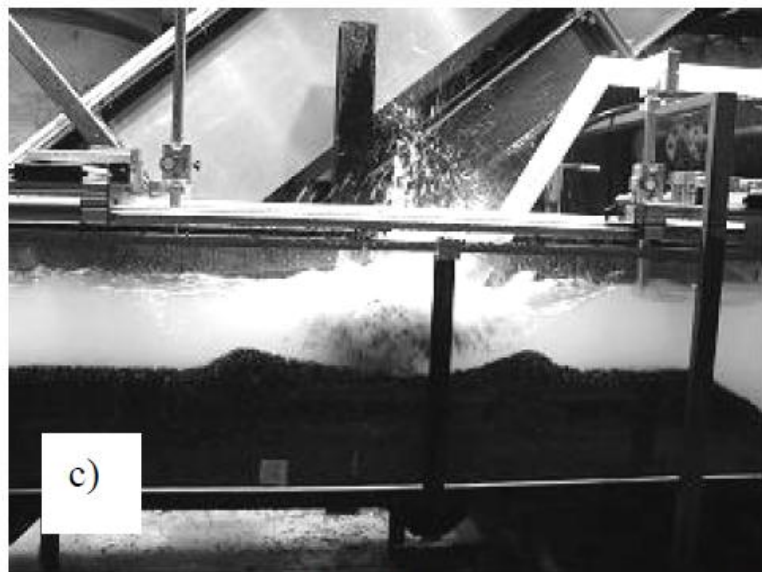
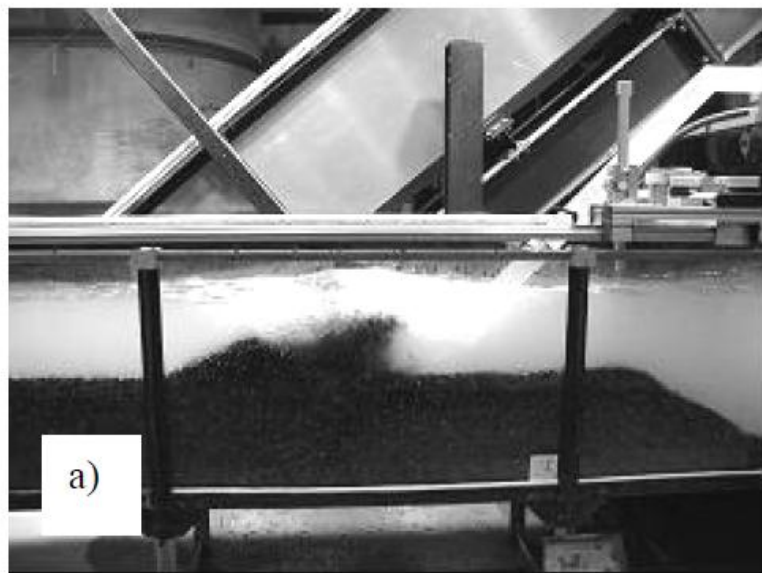


Figure 1. Photographs of plunge pool scour (45° jet angle) development (a) close to scour initiation, (b) close to scour end; view of a test with jet angle of 60° : (c) dynamic condition; (d) 'dry' conditions.

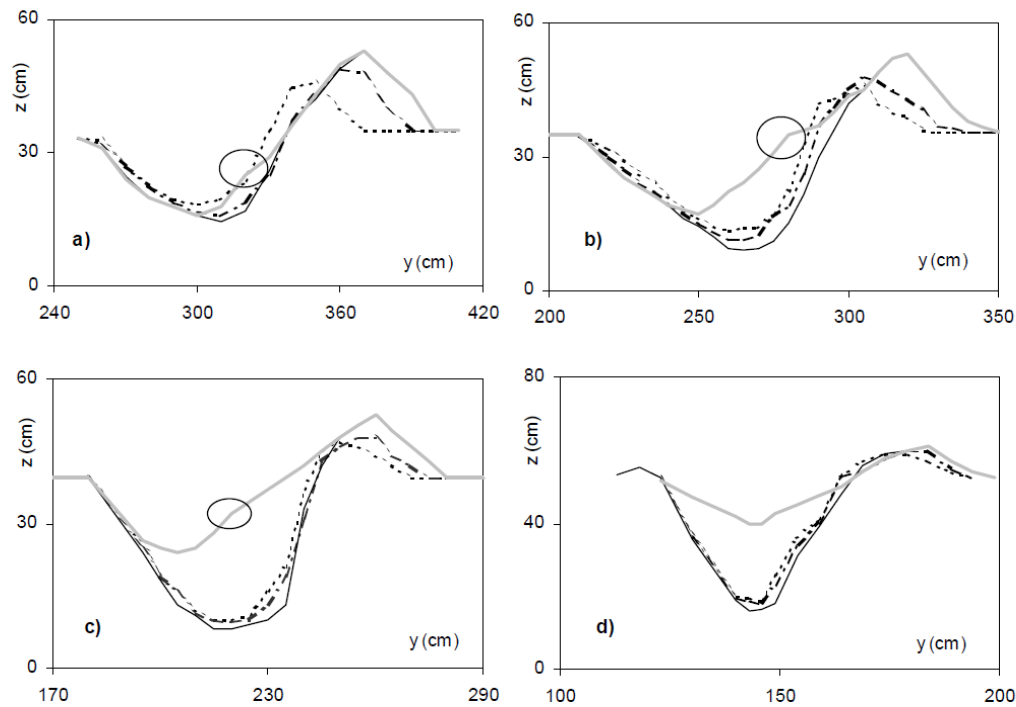


Figure 2. Scour profiles for dynamic and static conditions for (a) $\alpha=30^\circ$, Run BW30UB183, (b) $\alpha=45^\circ$, Run WW45UB21, (c) $\alpha=60^\circ$ Run WW60SC67, and (d) $\alpha=90^\circ$ Run BW90UC89 at times (....) 1, (---) 5, (—) 20 minutes and (—) 'dry' condition. Circles in (a) to (c) show the impact region of the falling suspended material when flow is stopped.

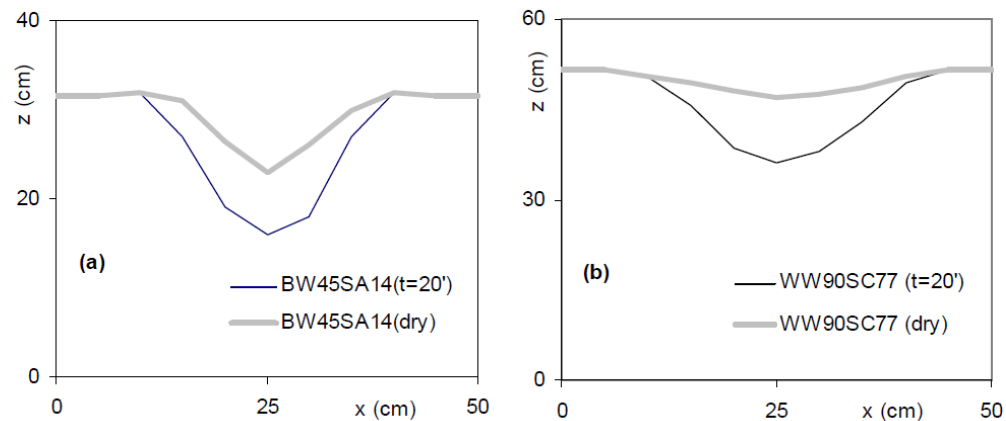


Figure 3. Cross-sectional scour profiles for (—) dynamic and (—) static conditions, (a) $\alpha=45^\circ$ (test BW45SA14) and (b) $\alpha=90^\circ$ (test WW90SC77).

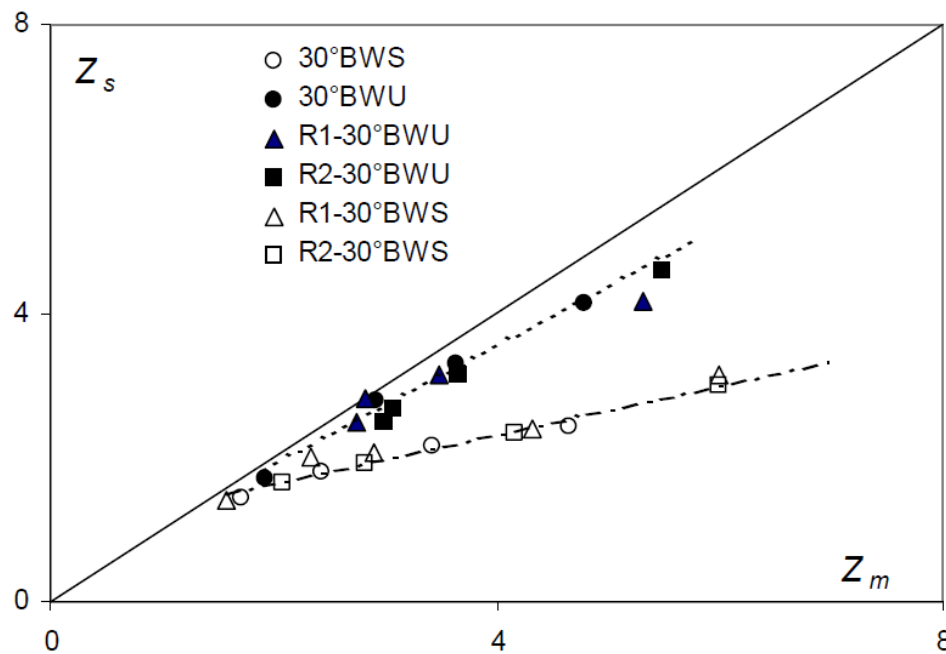


Figure 4. Shape effect for maximum static and dynamic scour depths, full symbols represent unsubmerged, open submerged impact conditions.

$$Z_s = 0.75Z_m^\varepsilon, \quad \varepsilon = E\alpha^{-0.75}, \quad 30^\circ \leq \alpha \leq 90^\circ$$

where the coefficient $E=14$ for unsubmerged, and $E=10$ for submerged jet flow.

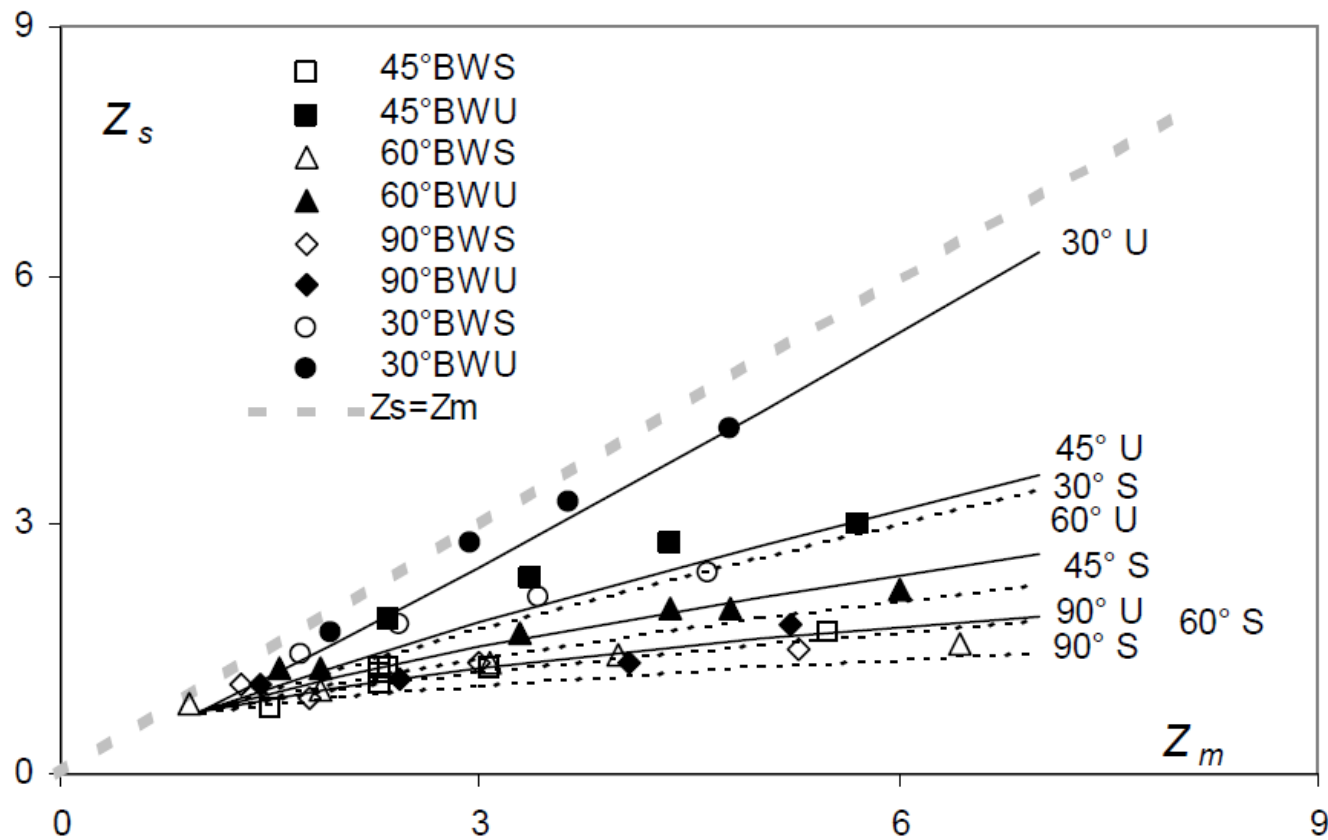


Figure 6. Regression of data for unsubmerged U and submerged S conditions for different angles α (eq.1).

$$Z_s = (0.06T + 0.7) \cdot \left[0.75 \cdot Z_m^{14\alpha - 0.75} \right] \cdot \zeta_{ZsT}$$

where Z_m is calculated with Eq. (1) and, for $\lambda > 3.0$ (2D case),

$$\zeta_{ZsT} = 1$$

whereas, for $\lambda \leq 1.50$ (3D case),

$$\zeta_{ZsT} = [0.879 + 0.274\lambda - 0.008\alpha^0] \cdot [1.165 - 0.026T]$$

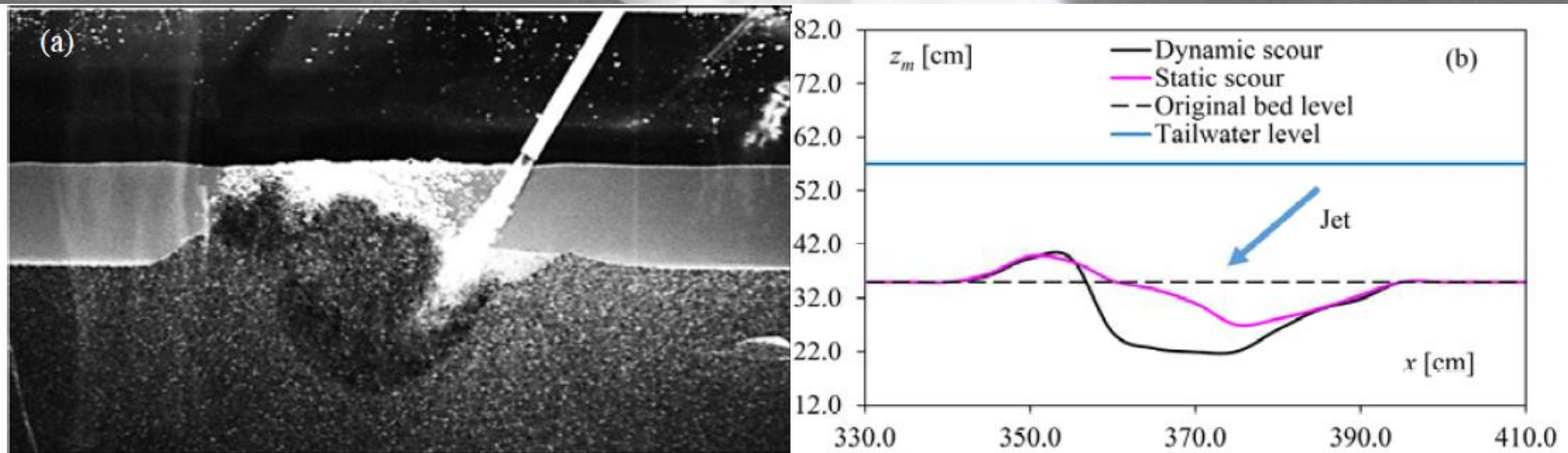


Figure 2. (a) Example of scour due to a single plunging jet. (b) Comparison between dynamic equilibrium and static scour profiles

2. Hydraulics of 3D Plunge Pool Scour

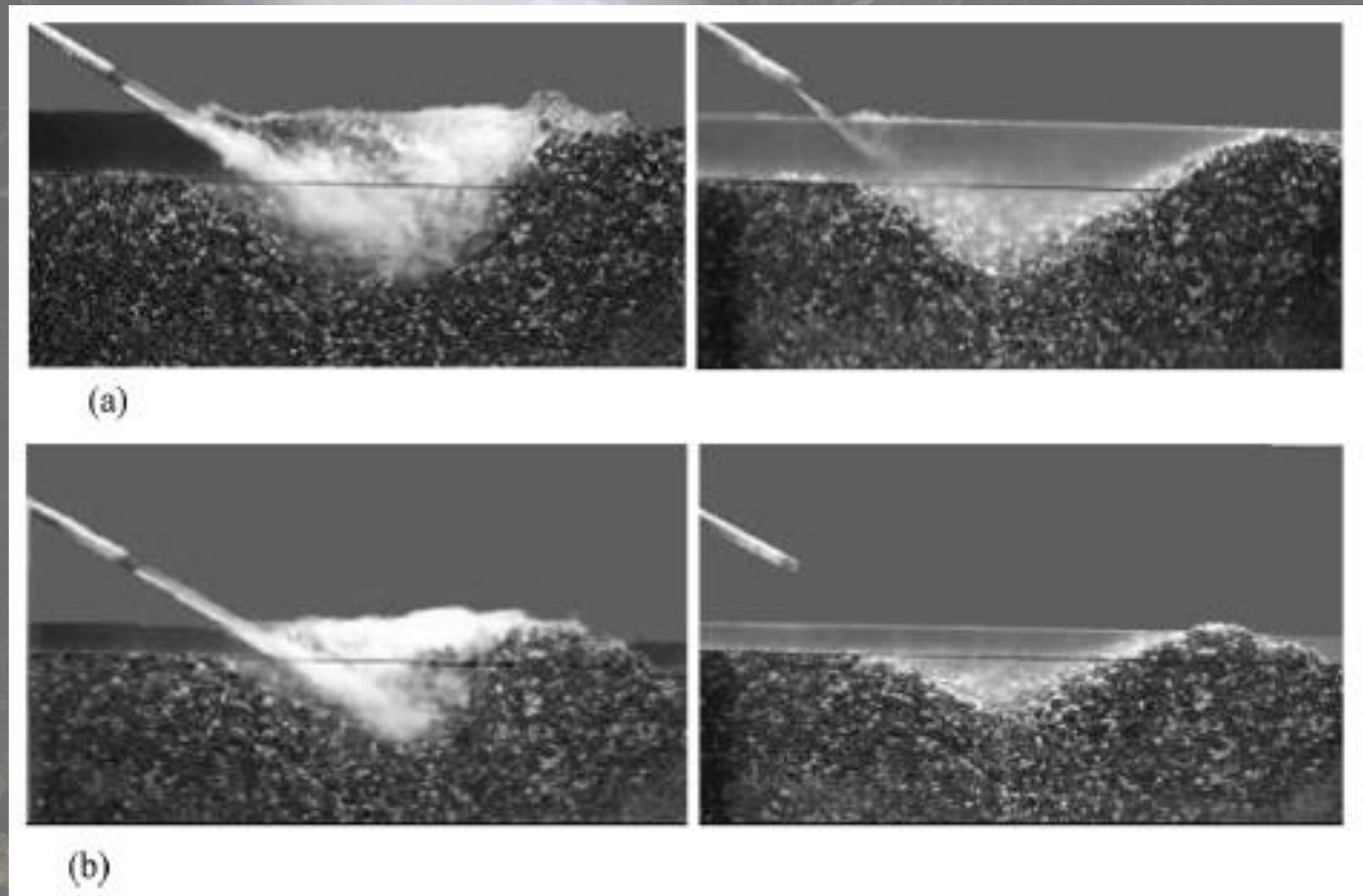


Fig. 10. Comparison between dynamic (left) and static (right) 3D scour holes for $\alpha=30^\circ$ and $T=$ (a) 5 and (b) 3. Note the large amount of suspended sediment in the dynamic scour holes.

COMPARISON WITH PROTOTYPE DATA

The various parameters needed for the analysis according to Pagliara et al (2004) were estimated based on Yildiz and Üzücek (1994) and Whittaker and Schleiss (1984), with the jet air content β calculated according to Ervine and Elsayw (1987) and a determining sediment size d_{90} of 0.30 to 2 m. It should be noted that this effect is relatively small and does not lead to a significant modification of the results.

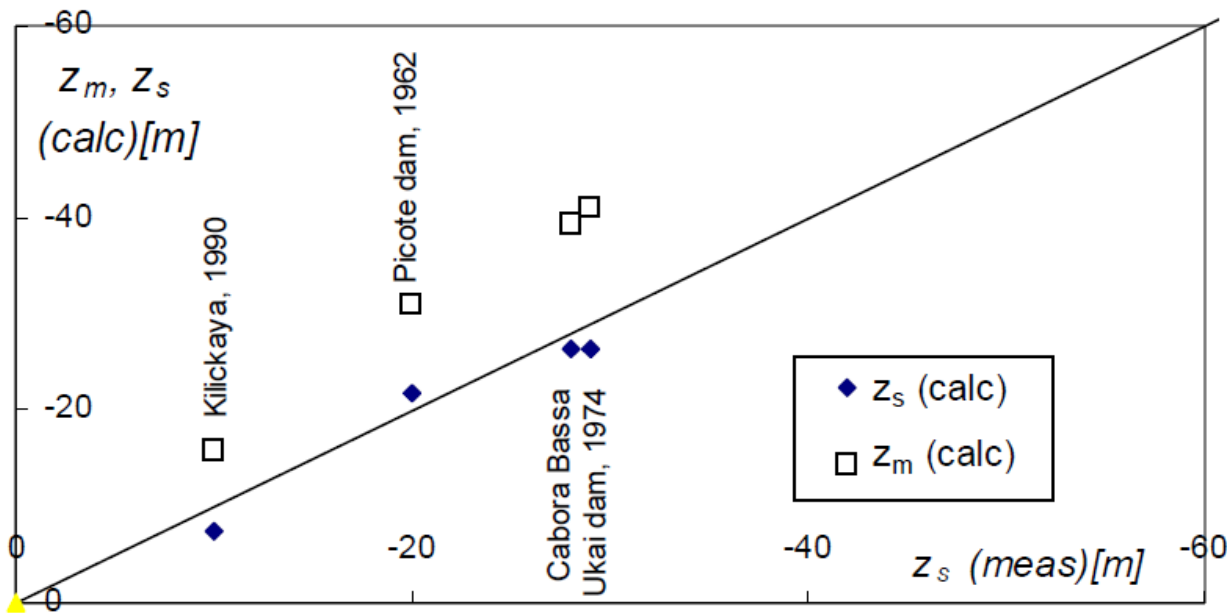


Figure 8. Comparison between prototype and calculated values of maximum plunge pool scour in prototype and laboratory

Stefano Pagliara
 Department of Civil Engineering, University of Pisa, I-56 100 Pisa, Italy
 Willi H. Hager
 VAW, ETH-Zentrum, CH-8092 Zurich, Switzerland
 Hans-Erwin Minor
 VAW, ETH-Zentrum, CH-8092 Zurich, Switzerland

d_{90} of 0.30 to 2 m.

3. Temporal evolution of plunge pool scour

The temporal development of plunge pool scour is important in order to understand the phenomena.

It is proved that the evolution is logarithmic, similar to that found for bridge pier and abutment scour.

3. Temporal evolution of plunge pool scour

The test program involved one nearly uniform sediment with a median diameter $d=0.00115$ m. Black water jets were produced with a high-precision pump attached to a piping system that was mounted on an adjustable carriage over the test channel (Fig. 1). The jet diameters were $D_{\text{test}}=0.0217$ and 0.0350 m, and the jet impact angles =30, 45, and 60° from the horizontal (Fig. 2). To allow for a close visualization of the scour hole, a half-model arrangement was applied.

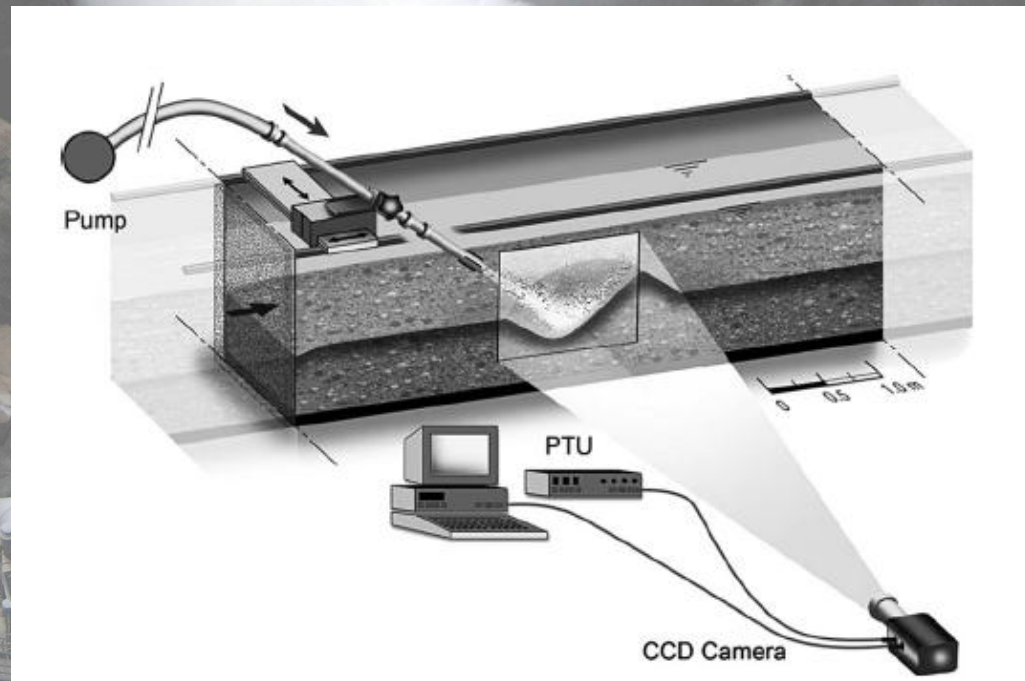


Fig. 1. Sketch of experimental setup

3. Temporal evolution of plunge pool scour

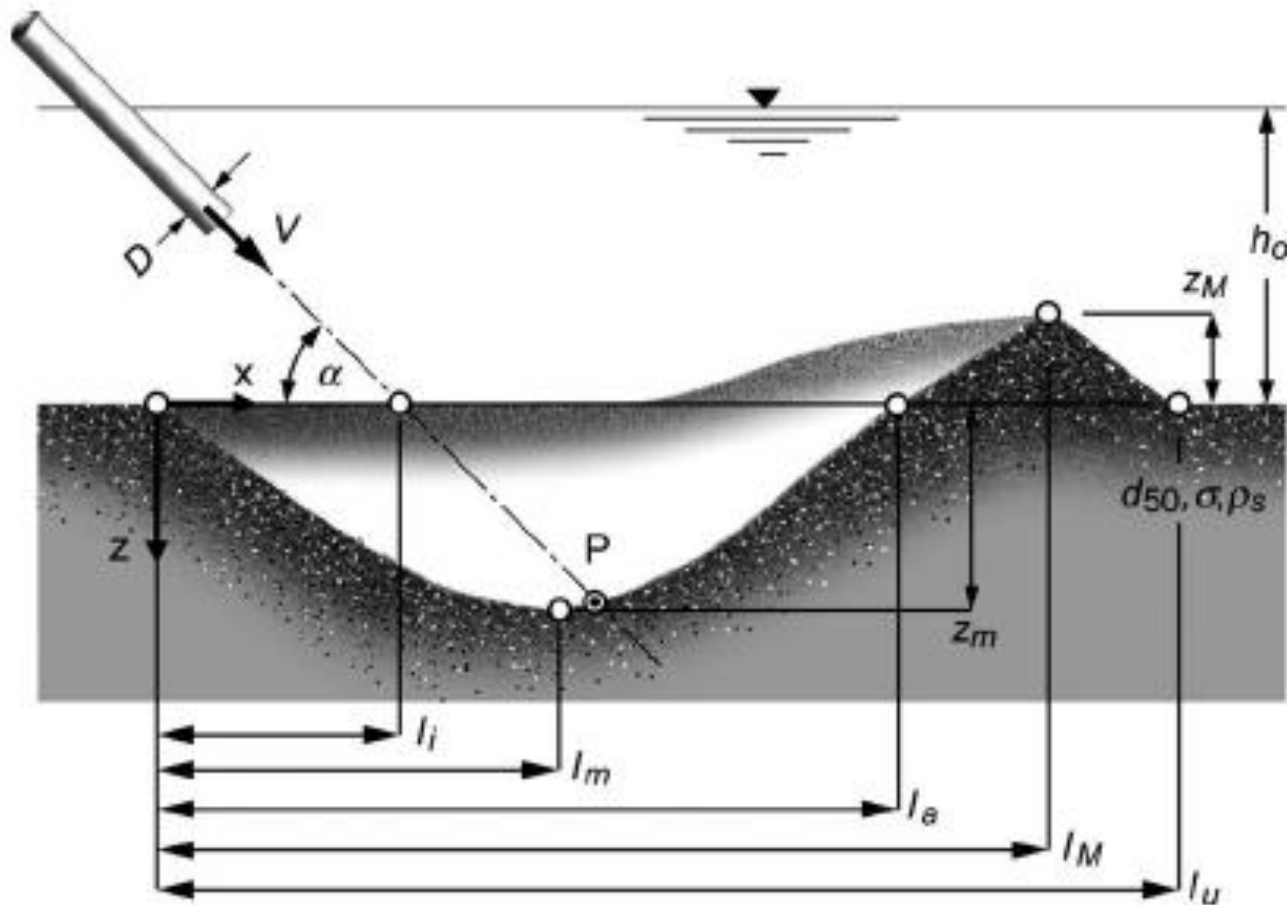
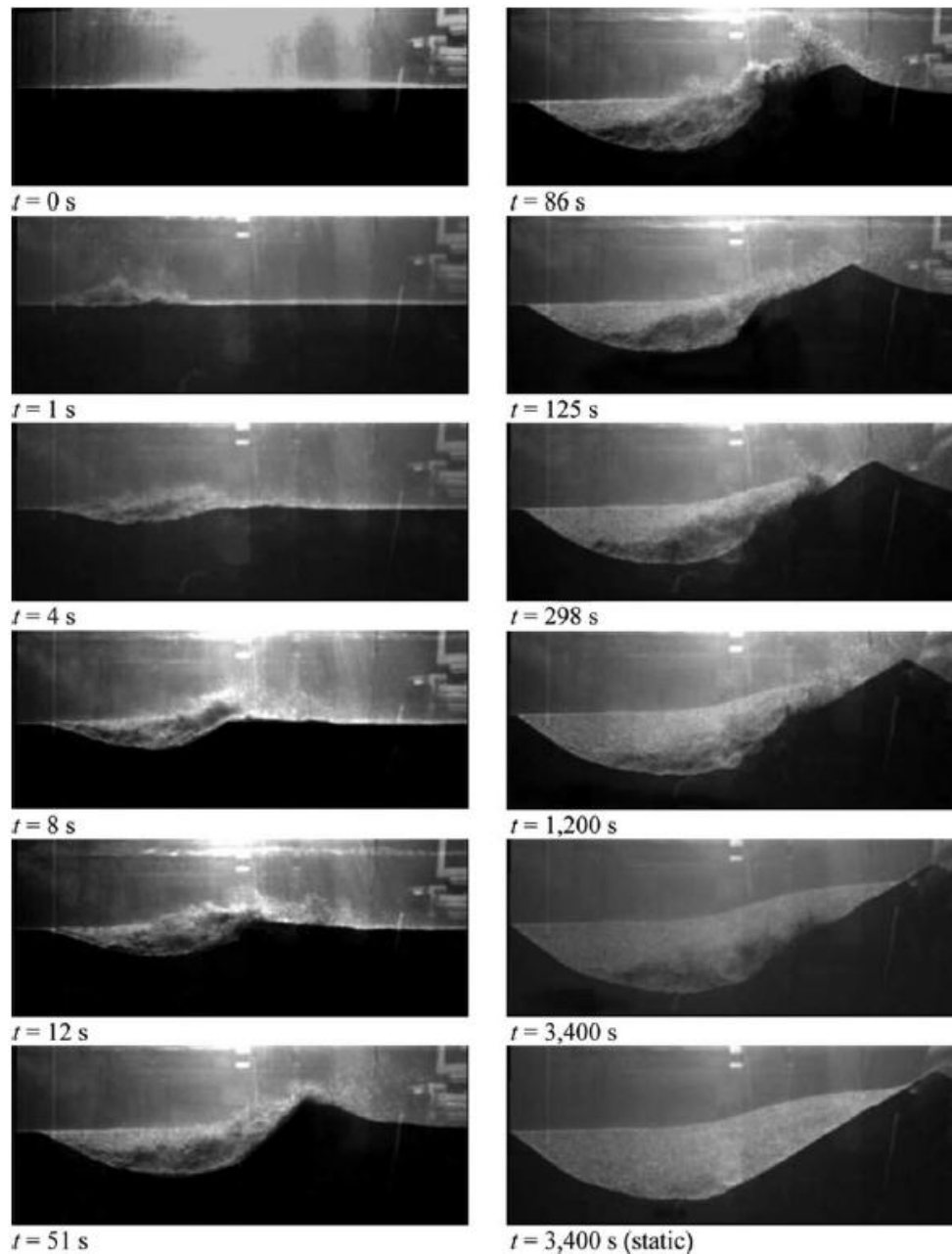


Fig. 2. Typical scour hole geometry, with notation



Developing phase (sx)
Developed phase (dx)

Fig. 3. Test T8A30S with $F_{d90}=33$, $\alpha=30^\circ$, S-jet, sequence of photos from $t=0$ to 3,400 s

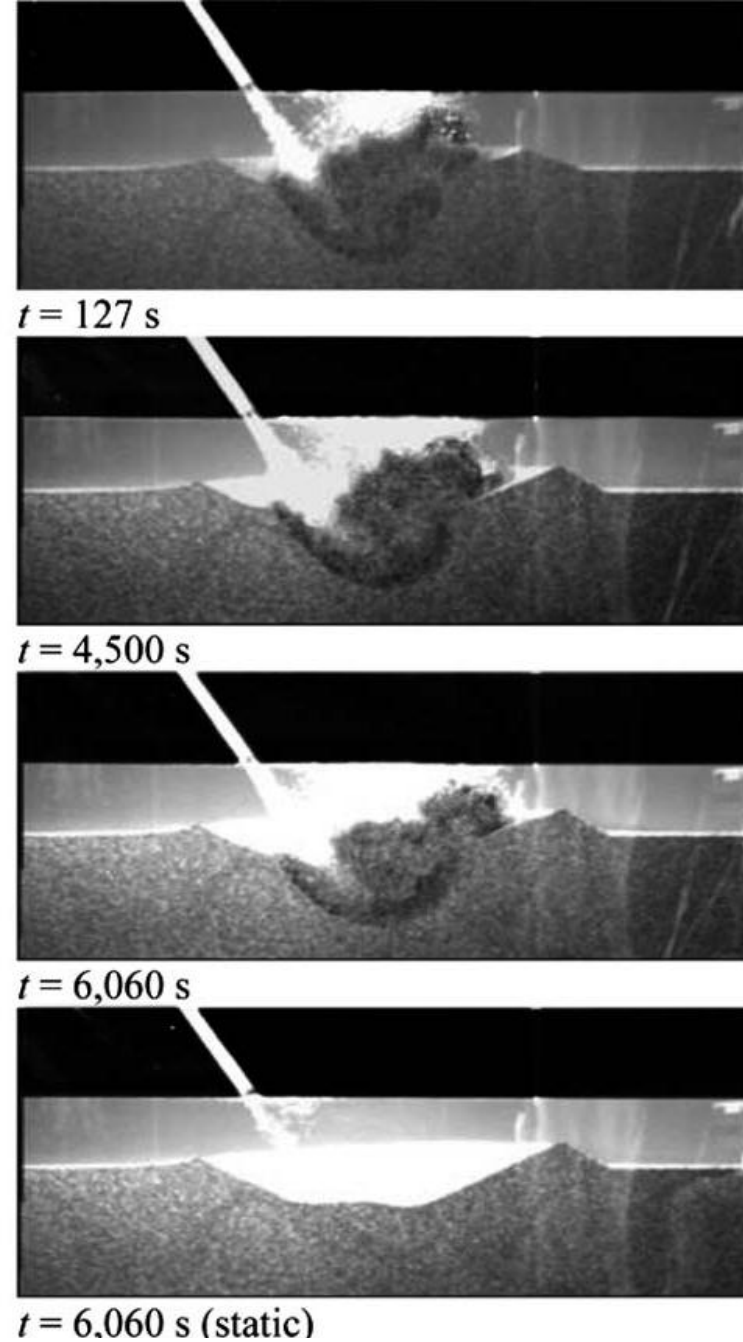
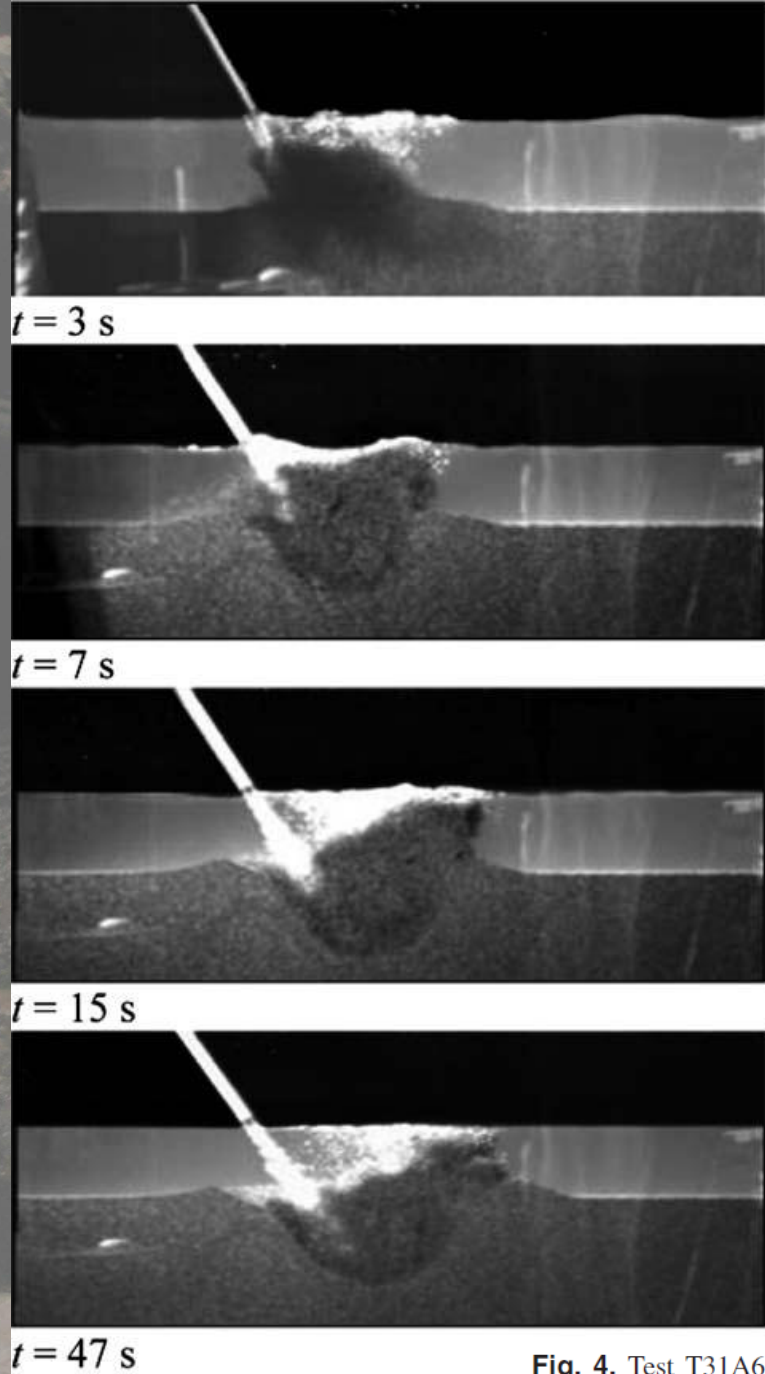


Fig. 4. Test T31A60U with $F_{d90}=27.8$, $\alpha=60^\circ$, U-jet, sequence of photos from $t=0$ to 6,060 s

Fig. 5. Dimensionless scour hole depth $Z_m(\log \tau)$ for: $\alpha=(a) 30^\circ$; (b) 45° ; and (c) 60° (light symbols=U-jets, full symbols=S-jets)

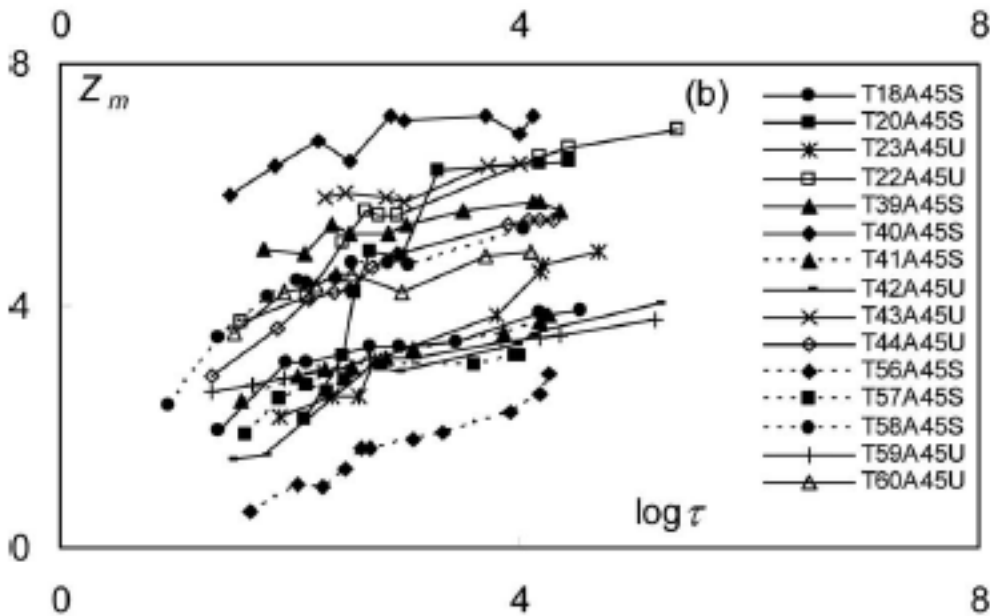
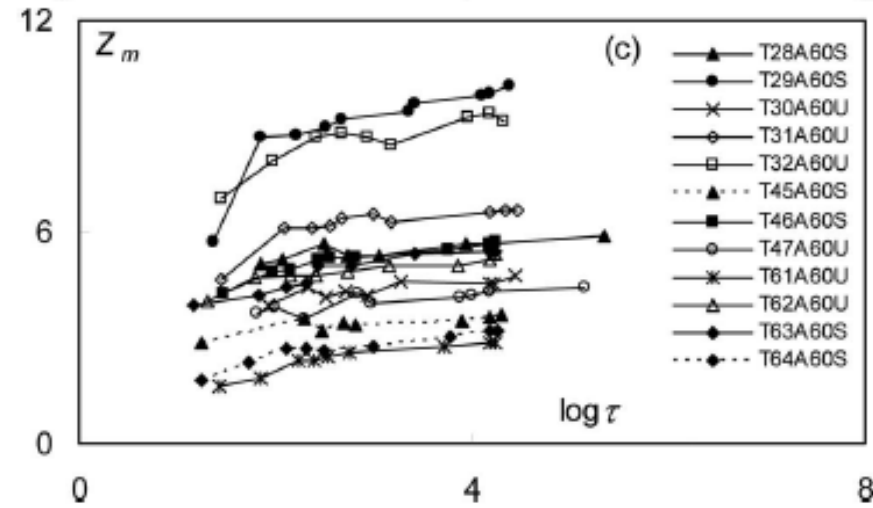
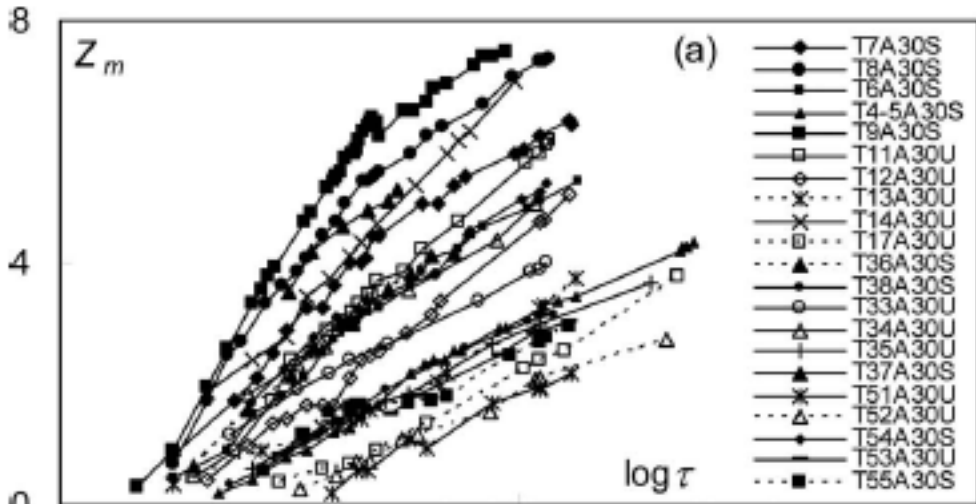


Fig. 5. Dimensionless scour hole depth $Z_m(\log \tau)$ for: $\alpha=(a) 30^\circ$; (b) 45° ; and (c) 60° (light symbols=U-jets, full symbols=S-jets)

$$\tau = (g' d_{90})^{1/2} \cdot t / D$$

$$g' = [(\rho_s - \rho) / \rho] g$$

$$Z_m = z_m / D$$

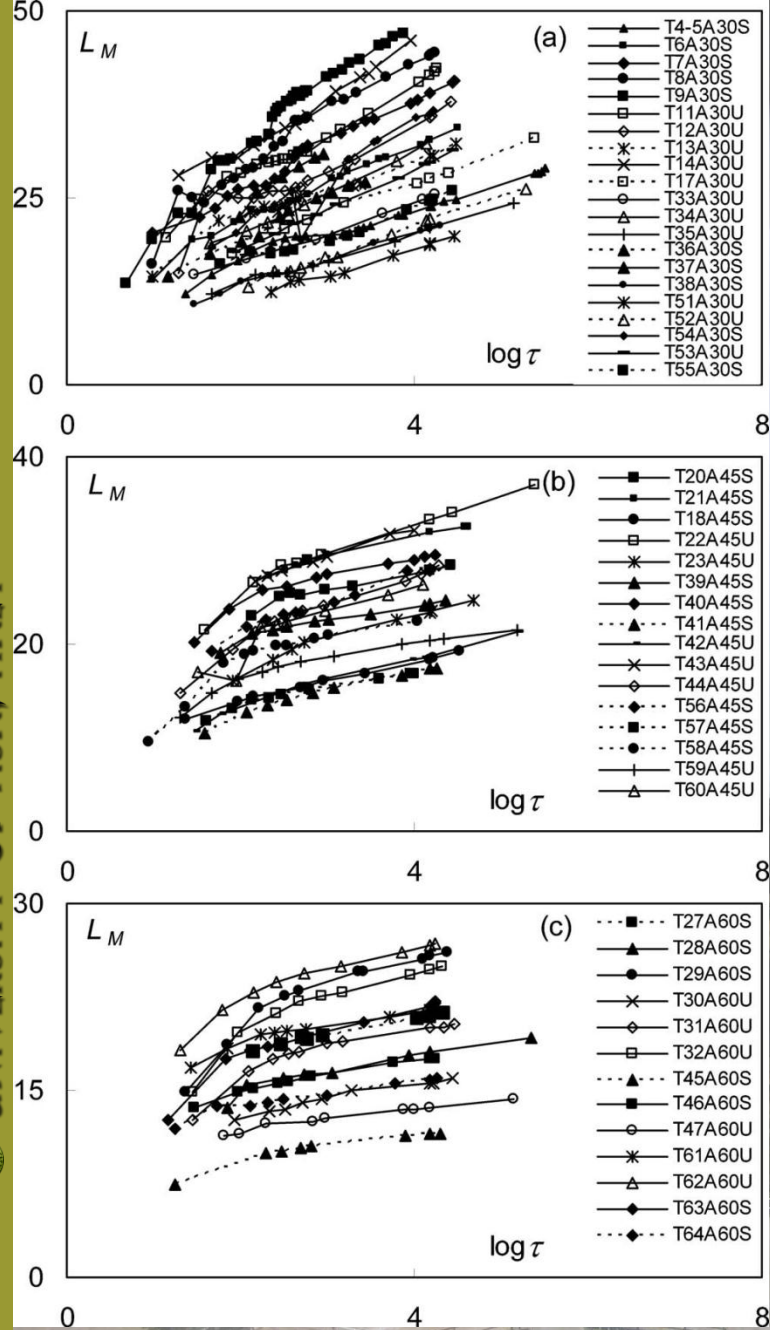


Fig. 6. Dimensionless location of maximum ridge height $L_M(\log \tau)$ for: $\alpha =$ (a) 30° ; (b) 45° ; and (c) 60° (light symbols=U-jets, full symbols=S-jets)

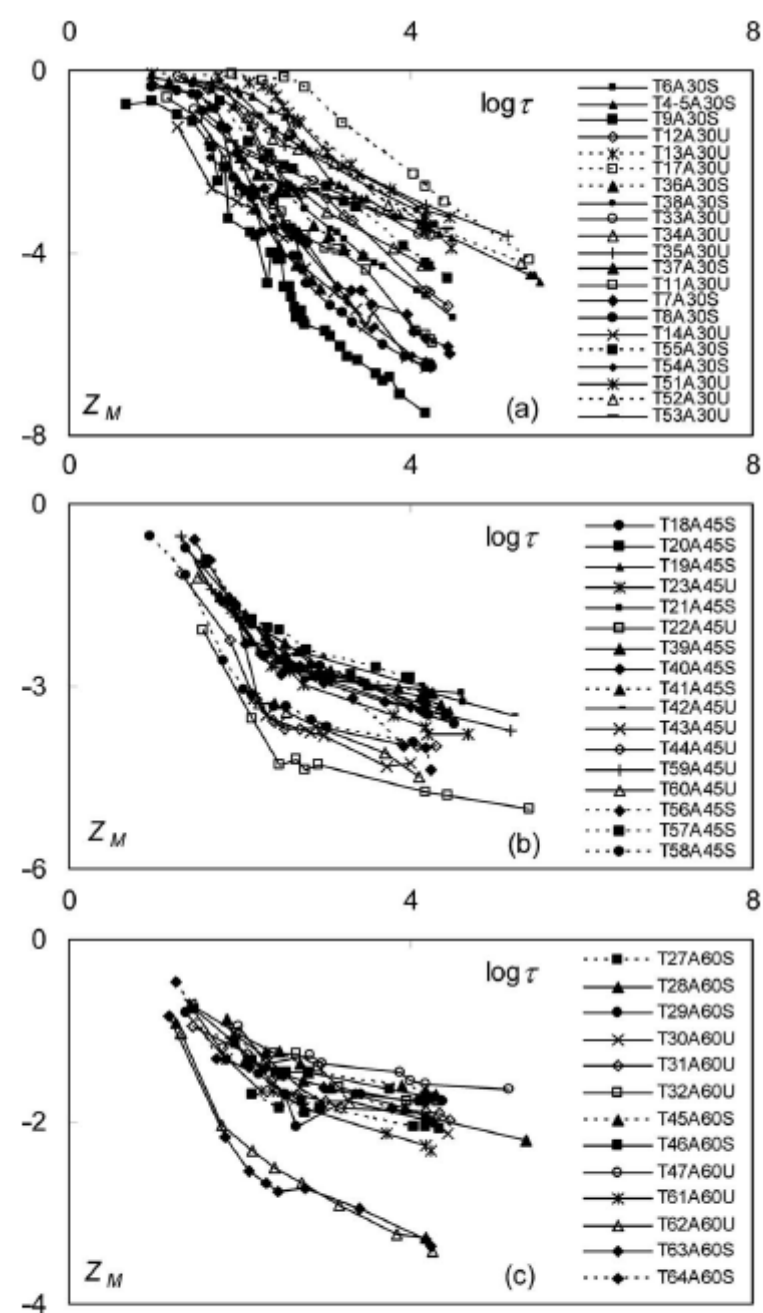


Fig. 7. Dimensionless ridge height $Z_M(\log \tau)$ for: $\alpha =$ (a) 30° ; (b) 45° ; and (c) 60° (light symbols=U-jets, full symbols=S-jets)

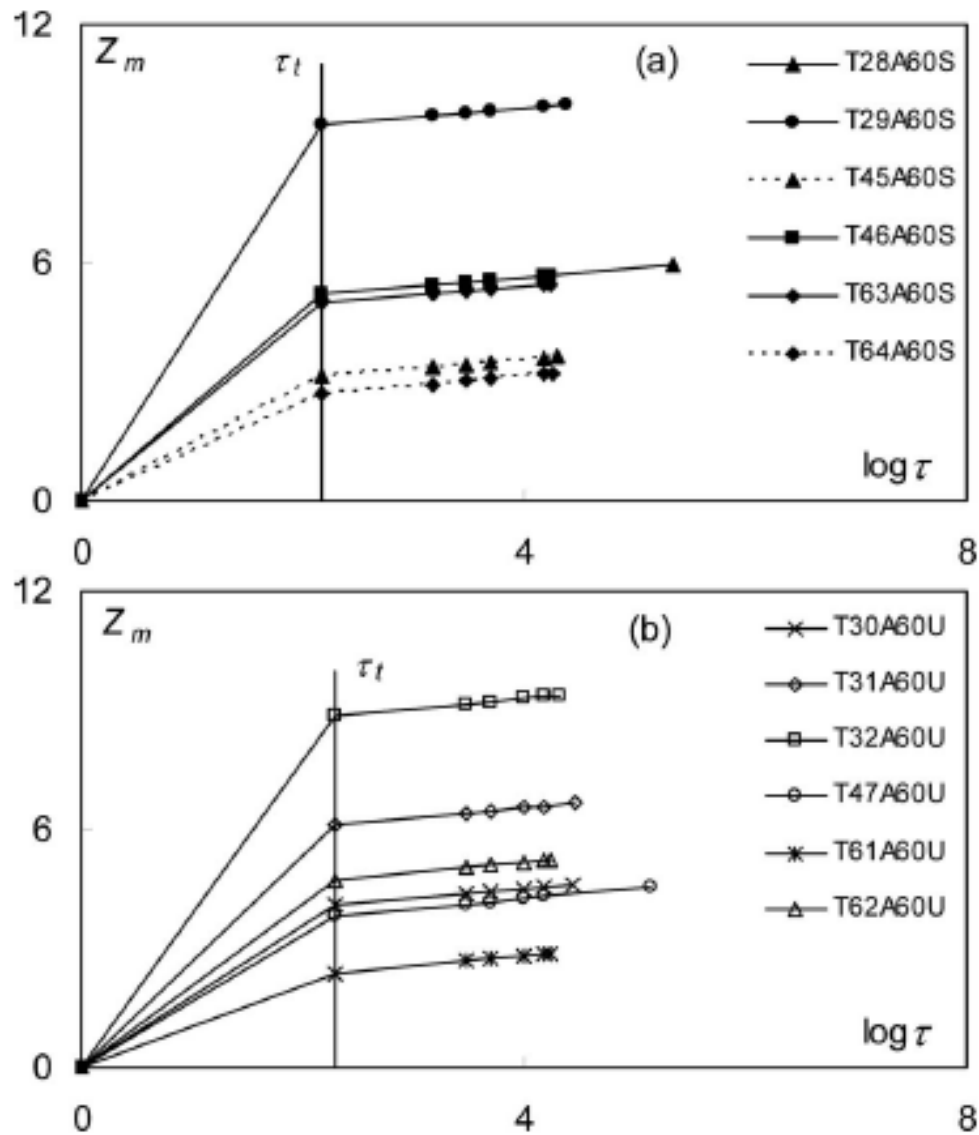


Fig. 10. $Z_m(\log \tau)$ for: $\alpha = 60^\circ$ and (a) S-jets; (b) U-jets

proposed the following expression to evaluate τ_t :

$$\tau_t = A_1^2(-0.78\alpha^2 + 51.68\alpha - 150) \quad (15)$$

where $A_1=1$ for submerged jets and $A_1=1.12$ for unsubmerged jets. Furthermore, they furnished two useful relationships by which it is possible to estimate the maximum scour depth at each instant of the evolution process. Namely, they proposed the following equations:

$$Z_m/Z_{mt} = \log \tau / \log \tau_t \quad (16)$$

valid for the developing phase ($0 < \tau < \tau_t$) and

$$Z_m(\tau) = 2000 \cdot A_1 \cdot \alpha^{-2.2} \cdot \log(\tau/15000) + Z_m(\tau=15000) \quad (17)$$

valid for the developed phase ($\tau \geq \tau_t$). Note that Z_{mt} is the non-dimensional scour depth at the transition time τ_t , whereas $Z_m(\tau=15000)$ is given by Eq. (11), as Pagliara et al. (2008b) showed that the equilibrium dynamic condition is reached for $\tau=15000$ in the tested range of parameters. Therefore, Eq. (17) can estimate both the developed phase up to the dynamic equilibrium configuration and the asymptotic trend characterizing the scour depth evolution for $\tau=15000$ and it is valid in the same range of parameters of the previous equations.

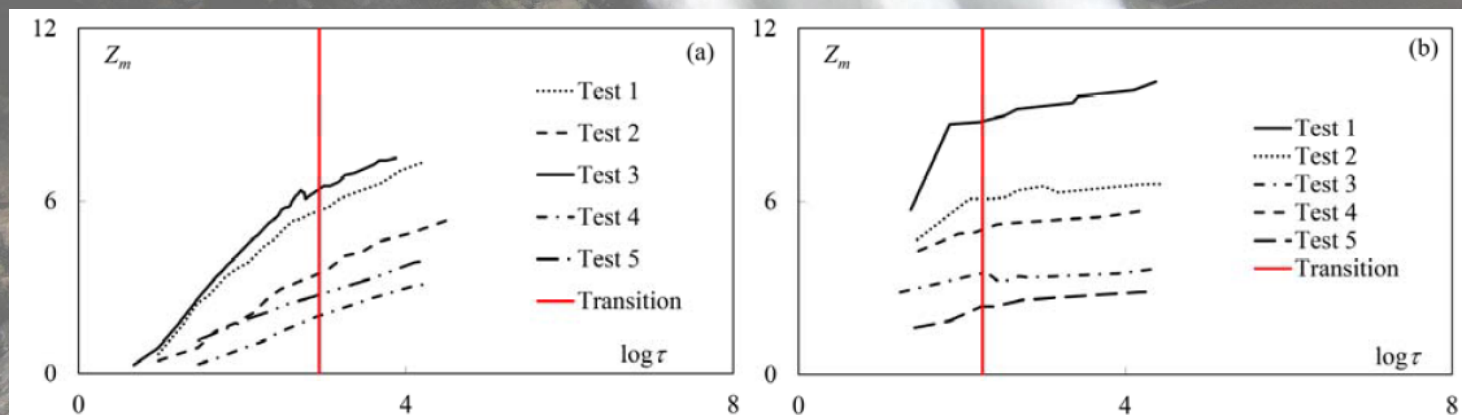


Figure 3. Non-dimensional scour depth evolution for jet inclination of (a) 30° and (b) 60°.

Multiple plunging jets: vertical and symmetric

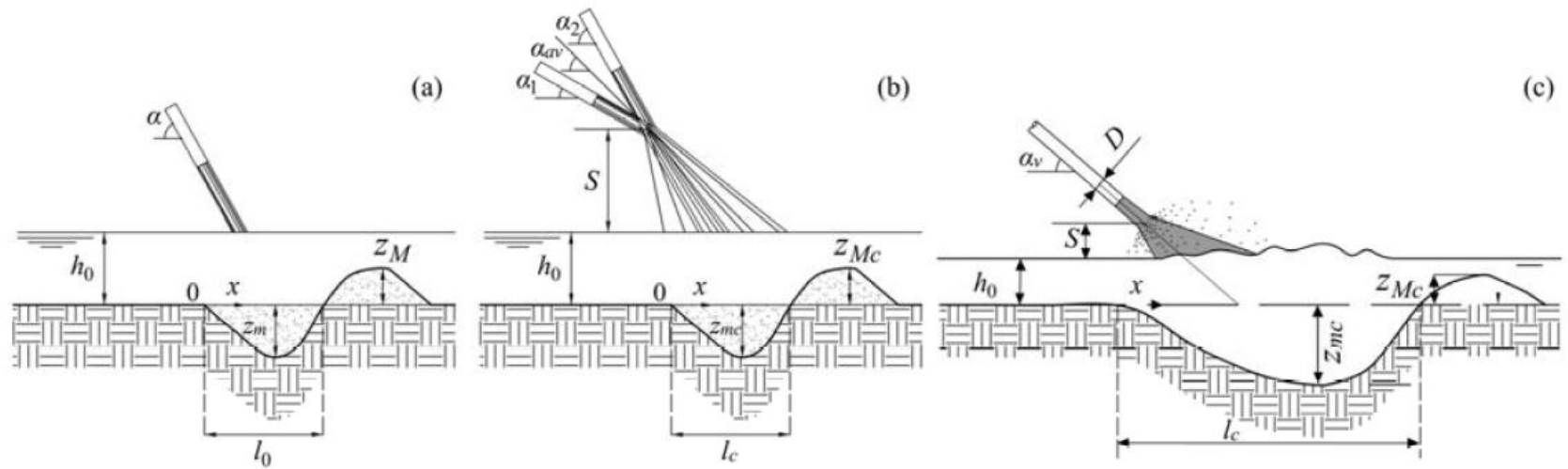


Figure 1. Diagram sketch of (a) single sub-vertical jet, multiple (b) vertical and (c) symmetric jets

$$\delta = S/D_{eq}$$



Figure 4. Pictures of multiple (a) vertical ($\alpha_1=30^\circ$ and $\alpha_2=60^\circ$) and (b) symmetric ($\alpha_c=30^\circ$ and $\alpha_v=60^\circ$) crossing jets

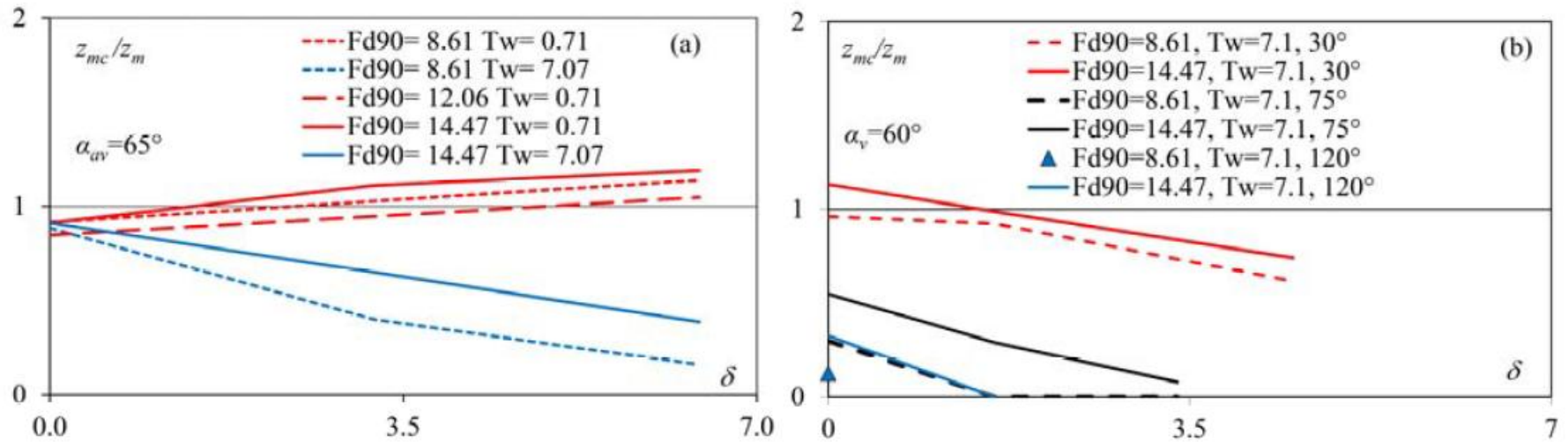


Figure 5. Comparison between single equivalent plunging jet and multiple (a) vertical and (b) symmetric crossing jets

Thank you





altro



$$\beta = Q_A / Q_W$$

Effect of Jet Air Content

The jet air content $\beta = Q_A / Q$ plays a significant role in plunge pool scour (Canepa and Hager 2003). It may either be analyzed with the black-water velocity $V_W = Q_W / (\pi D_W^2 / 4)$ with D_W as the black-water jet diameter, or with the air-water mixture velocity $V_{AW} = Q_W(1 + \beta) / (\pi D^2 / 4)$. The related Froude numbers are $F_{d90} = V / (g' d_{90})^{1/2}$ and $F'_{d90} = V_{AW} / (g' d_{90})^{1/2}$. The function $f_3(\beta)$ in Eq. (1) was determined with the parameter $Z_{m++} = Z_m / F'_{d90} = Z_m / [F'_{d90} \cdot f_2(\alpha)]$. Fig. 5 compares Z_{m++} for $\beta < 12$ with

$$f_3(\beta) = (1 + \beta)^{-m} \quad (3)$$

where $m = 0.75$ for the unsubmerged and $m = 0.50$ for the submerged jet configuration, respectively. The effect of jet air content is (slightly) larger for unsubmerged than for submerged jets. The provisional equation for the maximum scour depth Z_m due to an air-water mixture jet thus reads

$$Z_m = z_m / D_e = -0.38 \sin(\alpha + 22.5^\circ) \cdot F'_d \cdot (1 + \beta)^{-m} \quad (4)$$

$2 < F'_d < 40, \quad 30^\circ \leq \alpha \leq 90^\circ$

This relation includes the effects of equivalent jet diameter D_e for noncircular jets, the jet impact angle α , the mixture velocity V_{AW} , the relative density times the gravitational acceleration $g' = [(\rho_s - \rho) / \rho]g$ between sediment and fluid phases, the grain size d_{90} , and the jet air content β . Fig. 6 compares the present observations with Eq. (4) for the 200 data sets of Series I for both submerged and unsubmerged jet flow conditions. Note that the white-water jets were almost uniformly aerated, in contrast to typical prototype jets with a black-water core and increasing air concentration from the jet axis towards the jet surface. This effect was considered relatively small. Both the externally aerated high-speed jet and jet impact geometries deviating strongly from the circular cross section must be investigated separately to confirm the present result, however.

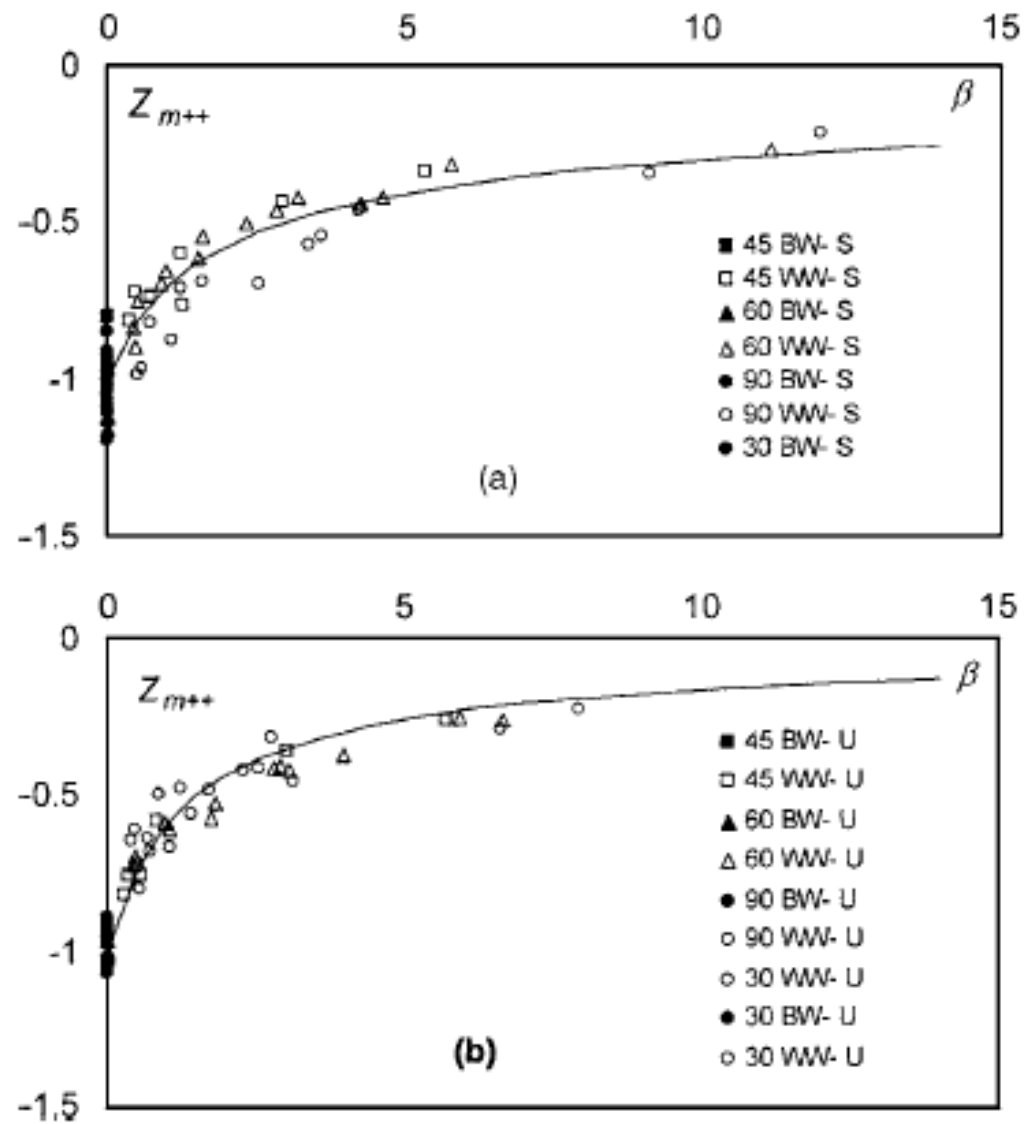


Fig. 5. Effect of jet air content β on maximum scour depth Z_{m++} for (a) submerged (S) and (b) unsubmerged (U) flow conditions, (—) Eq. (3)